IJIRSET
International Journal of Innovative Research in
SCIENCE | ENGINEERING | TECHNOLOGY

e-ISSN: 2319-8753 | p-ISSN: 2347-6710

INTERNATIONAL JOURNAL OF INNOVATIVE RESEARCH

IN SCIENCE | ENGINEERING | TECHNOLOGY

Volume 13, Issue 5, May 2024

ISSN INTERNATIONAL STANDARD SERIAL NUMBER INDIA

Impact Factor: 8.423

9940 572 462 | 6381 907 438 | ijirset@gmail.com | www.ijirset.com

International Journal of Innovative Research in Science, Engineering and Technology (IJIRSET)

|e-ISSN: 2319-8753, p-ISSN: 2347-6710| www.ijirset.com | Impact Factor: 8.423| A Monthly Peer Reviewed & Refereed Journal |

|| Volume 13, Issue 5, May 2024 ||

| DOI:10.15680/IJIRSET.2024.1305357 |

A Novel ANFIS Controller Based Distributed Power Flow Controller for Grid Interfaced Hybrid System

Rudra Thakkar, Mr. Ruchit Soni, Dr. Sweta Shah

P.G. Student, Department of Electrical Engineering, Indus University, Ahmedabad, Gujarat, India

Associate Professor, Department of Electrical Engineering, Indus University, Ahmedabad, Gujarat, India

Associate Professor, Department of Electrical Engineering, Indus University, Ahmedabad, Gujarat, India

ABSTRACT: A novel Adaptive Neuro-Fuzzy Inference System (ANFIS) controller is proposed in this project as a solution for the control of grid-interfaced hybrid systems. The aim is to develop a Distributed Power Flow Controller (DPFC) that can effectively manage power flow and improve the stability of the system. The proposed ANFIS-based DPFC is designed to handle complex non-linear dynamics of hybrid systems and provide real-time control strategies. The performance of the proposed controller is evaluated through simulation studies and compared with conventional controllers to demonstrate its effectiveness in maintaining stability and improving the overall performance of the grid-interfaced hybrid system. The performance of the proposed method and conventional method results compared in terms of total harmonic distortion and evaluated by using MATLAB/Simulink software.

I. INTRODUCTION

The current situation has seen a sharp rise in the need for electrical energy. Pollution and greenhouse effects result from the use of conventional power generation methods, such as gas, coal, and nuclear power plants [1]. Non-conventional sources are crucial to the current energy generation systems' ability to meet electrical demand while resolving environmental issues [2]. The primary benefits of these renewable energy sources are their lack of pollution, low maintenance costs, and affordability. Zhouyang Ren served as the associate editor who oversaw the manuscript's review and gave it approval for publication. Although there are more renewable energy systems on the market, they are still more important than all wind and solar energy systems due to their straightforward design, accessibility to environmental resources, and extremely effective operating conditions [3]. In hybrid systems, photovoltaic and wind energy systems are important energy sources [4]. When compared to other renewable energy sources, photovoltaic systems are among the most practical renewable energy sources [5]. Photovoltaic systems are very expensive to install and are not naturally stable in terms of time, location, weather, or season. Variations in the weather have an impact on the solar system's output [6]. As such, MPPT techniques were applied in order to maximize output and boost solar panel efficiency [7]. Wind energy systems are another important renewable energy source for PV systems, depending on the natural conditions that are present. The amount of wind that exists in the environment determines the ratio of electrical energy generation [8]. The outputs produced by wind systems are impacted by variations in the weather [9]. Therefore, MPPT techniques are used to maximize output and boost the wind system's efficiency. The system needs to stay in sync with the grid. In order to match the frequency levels and system rates, the solar system was connected to a voltage source inverter. The control diagram for the inverter was created using a general PWM technique, and the reference signals were selected based on grid parameters [10]. Electric power systems nowadays are big and intricate. In a networked power system, both territory recurrence and tie-line power exchange occur when a power burden request varies randomly. Without control, it is hard to keep age and burden in balance [11]. Accordingly, a control framework is essential to reduce the effects of irregular load variations, maintain recurrence at the standard worth, and illustrate the fundamentals of a reorganized power system [12].

1.1 Index Terms

Distributed power flow controller, fuzzy logic controller, grid interconnected, PV system and wind energy system, ANFIS controller.

|e-ISSN: 2319-8753, p-ISSN: 2347-6710| www.ijirset.com | Impact Factor: 8.423| A Monthly Peer Reviewed & Refereed Journal |

|| Volume 13, Issue 5, May 2024 ||

| DOI:10.15680/IJIRSET.2024.1305357 |

1.2 Literature review

J. B. Holm-Nielsen, S. Xavier, S. Padmanaban, U. Govindarajan, V. K. Ramachandaramurthy, A. Rajagopalan, N. Pachaivannan, U. Sowmmiya, and S. K. Periasamy One easy preventative measure to shield the environment from pollution and resource depletion is cleaner production. Additionally, it is intended to reduce waste and maximize the use of natural resources. Using a photovoltaic (PV) system, solar energy is a renewable resource that can be transformed into electricity. This article analyzes the reasons and obstacles for PV adoption by various Indian citizen groups, providing insights into the implementation of solar PV systems from an interdisciplinary perspective. To find out how people felt about solar PV energy systems and how acceptable they were to the general public, a survey was done. The survey data was combined and analyzed from a variety of angles, and the end product divides the research findings into socioeconomic, technical, and human components. The results of cross-cultural, comparative, and mixed-method research were combined using biplot interpretation, Dendrogram diagrams, and structural equation modeling (SEM). To interpret the data, statistical tools like "IBM-SPSS Amos" and "R" language programming were also utilized. The article ends by outlining the obstacles that prevent more retrofitting interventions and offering potential solutions in the form of laws and policies that could help remove these obstacles and advance solar energy in India.

The following people: A. Annam, A. M. Vetrichelvan, L. Mihet-Popa, R. M. Elavarasan, G. Shafiullah, S. Padmanaban, N. M. Kumar, and J. B. Holm-Nielsen Nowadays, there is a lot of interest in clean and environmentally friendly energy harvesting since it is essential to reaching the Sustainable Development Goals (SDGs), accelerates social progress, and raises living standards. With 1.353 billion people, India is the second most populous country in the world and one of the biggest users of fossil fuels, which contributes to global warming. Up until 2050, population growth is expected to continue, and as a result, rapid industrial growth will coincide with an increase in energy demand in the coming decades. The National Institute for Transforming India (NITI) Aayog and the Ministry of New and Renewable Energy (MNRE) are collaborating to help the Indian government reach its goal of 175 GW of renewable energy. In an effort to meet future energy demand, several Indian states are currently expanding their capacity for renewable energy. The review paper goes into great detail about the three Indian states that led the country's production of renewable energy: Karnataka, Gujarat, and Tamil Nadu. A detailed discussion of the global energy scenario was held, contrasting it with India. Additionally, since the difficulties faced by other countries are similar to India's, the policies of the Indian government and the obstacles to the growth of renewable energy generation are examined in detail in order to promote renewable energy generation both nationally and internationally. This study examined the nation's prospects for renewable energy and was conducted with the intention of assisting academics, researchers, and policymakers in the country by providing an understanding of the current state of renewable energy in the nation.

P. Sanjeevikumar, S. Kumar, R. K. Saket, D. K. Dheer, and J. B. Holm-Nielsen. An extensive survey on the electrical network system's reliability evaluation is presented in this study. The article discusses how the reliability of the electrical power system (EPS) is affected by the integration of new and renewable energy sources, such as energy storage systems, electric vehicles, solar power, and wind. When these renewable energy sources are combined with the traditional electrical power system, there are advantages and disadvantages to their effects. Still, the benefits outweigh the drawbacks because it comes with limitless, free, and affordable resources. Recent studies show that the probabilistic and reliability analyses of EPS are influenced by the uncertainties surrounding renewable energy resources. Energy storage systems, microgrids, onshore and offshore wind farms, and other high voltage grids are all included in EPS. It also includes the parts of the power systems that are prone to failure. The handling techniques of uncertainty parameters in generation, transmission, and distribution systems are discussed in order to achieve these goals. There is also a brief discussion of the integration of energy storage systems, wind energy systems, and electric vehicles for reliability assessment. The scope of a new research area for researchers studying the reliability assessment of integrated power systems using renewable energy is also presented in this study.

In rural areas, the lack of an electric power grid network has made the production of hybrid power from renewable energy sources (RESs) like wind and solar photovoltaic (PV) inevitable (I. Masenge and F. Mwasilu). Large-scale energy storage system (ESS) deployment is required to meet load demands due to the RESs's reliable power supply, which comes with a hefty investment cost. Finding the best hybrid system design is essential to lowering the ESS requirements. The battery energy supply system (ESS) must be optimized in order to effectively reduce system costs. This paper suggests using Mixed Integer Linear Programming (MILP) to model and coordinate control a hybrid solar PV-wind power generation system along with the best BESS. The goal of the proposed scheme is to ensure that the voltage and system frequency at the Point of Common Coupling (PCC) remain constant, thereby preserving power flow

|e-ISSN: 2319-8753, p-ISSN: 2347-6710| www.ijirset.com | Impact Factor: 8.423| A Monthly Peer Reviewed & Refereed Journal |

|| Volume 13, Issue 5, May 2024 ||

| DOI:10.15680/IJIRSET.2024.1305357 |

between DC-AC buses. The MATLAB/Simulink simulation results verify the superior performance of the suggested scheme.

A. Suman, in extremely climate-vulnerable countries like Nepal, renewable energy is essential for both mitigating the effects of climate change and adapting to them. This study examines different kinds of renewable energy technologies and discusses their current state, adoption potential, connection to climate change, and roles in Nepal in terms of mitigation and adaptation. To reduce the effects of and prepare for climate change, Nepal has implemented micro-hydro projects, solar power, upgraded cooking stoves, biogas technology, upgraded water mills, and wind energy. Nepal has increasing possibilities for the development of better cooking stoves and renewable energy sources including biogas, solar, wind, and hydropower. Traditional energy sources provide for over 70% of Nepal's energy usage, with renewable energy making up the remaining 3%. Reduced greenhouse gas emissions and improved carbon sequestration have resulted from the steady growth in the usage of renewable energy. Nepal has decreased emissions by 221,129 tCO2e between 2017 and 2018 by using renewable energy technology. Nepal's second Nationally Determined Contribution aims to reduce CO2 emissions by 23% by 2030 by using biogas and better cooking methods, while increasing the country's energy consumption from renewables by 15%. In addition, a major surge in the use of renewable energy has emerged as a key tactic for the social, health, and economic sectors to adapt to climate change. This has led to time savings, the creation of new revenue streams, better health and educational outcomes, the creation of local job possibilities, and the development of social capital. At the municipal, state, and federal levels, there are major advantages to utilizing renewable energy sources to mitigate CO2 emissions and adapt to climate change. This study, which has worldwide consequences, suggests that the government of Nepal concentrate its efforts on reviewing its energy policies in order to solve concerns related to local energy consumption and climate change by leveraging renewable energy resources locally.

L. Varshney, P. Sanjeevikumar, R. Saket, S. Kumar, and A. S. S. Vardhan. Using data from a self-excited induction motor functioning as a generator, the research offers the performance analysis-based dependability estimation of a self-excited induction generator (SEIG) using the Monte-Carlo simulation (MCS) approach. The capacity of a SEIG to strengthen the system's inadequate frequency and voltage control will determine how widely accepted it is. Because the magnetizing current for the grid-connected induction generator is taken from the grid, the grid becomes weakerIn contrast, an external capacitor arrangement is used to provide reactive power supply in the SEIG stand-alone operation. In the stand-alone version of SEIG, this capacitor arrangement is linked across the stator terminals. Voltage build-up and improved power factor are the two functions of the capacitor. For this reason, the research focuses on determining the lowest value of capacitor needed for SEIG excitation in isolated mode applications, such as standalone wind power production. Various SEIG parameters have been considered in the evaluation of the SEIG performance characteristics. We then compare and find that the findings of the simulation and the experiment are good. The failure and success rates of the SEIG excitation during laboratory experiments are then taken into account when estimating the SEIG dependability using the MCS approach. In the end, various wind speeds are taken into account while evaluating the SEIG dependability.

K. Okajima, M. Yoshita, Y. Hishikawa, and M. Seapan. Experiments and numerical simulations based on a single diode model are used to study the temperature and irradiance dependences of the current at maximum power (I_{mp}) and the voltage at maximum power (V_{mp}) of crystalline silicon photovoltaic (PV) systems. The experimental Imp is demonstrated to be almost constant for temperature fluctuation at given irradiances, which is consistent with the modeling findings, which reveal that the range of parameters represents typical commercial crystalline silicon PV devices and are within ±0.02%/K over 273.15–343.15 K (0–70 °C). The simulation findings show that the Imp/G is approximately constant within ±1.3% over the irradiance range between 0.5 and 1.2 kW/m2, which is consistent with the experimental Imp being roughly proportional to irradiance (G) at fixed temperature. A novel formula for the temperature adjustment of Vmp is suggested in light of these findings. The temperature coefficient and diode characteristics do not need to be known in advance. Confirming the validity of the method, the Imp − Vmp curves, which are measured outdoors and adjusted to 25 °C using the formula, showed high consistency within ±0.13% over many days. The temperature adjustment of Vmp allows for an accurate estimation of the maximum power, Pmax. These findings are helpful in assessing the performance of PV devices made of crystalline silicon by utilizing the Imp and V_{mp} values, which are measurable while the devices are operating at maximum power point tracking (MPPT).

F. Mebrahtu, B. Khan, P. K. Maroti, Z. Leonowicz, O. P. Mahela, P. Sanjeevikumar, and H. H. Alhelou Industrial loads have power quality issues like harmonics because of the abundance of non-linear loads and power electronics devices in the power system. Harmonics cause appliances to overheat and shorten their lifespan. In order to reduce harmonics for non-linear loads, this work introduces the 3-Ω space vector pulse width modulation (SVPWM) and shunt active

|e-ISSN: 2319-8753, p-ISSN: 2347-6710| www.ijirset.com | Impact Factor: 8.423| A Monthly Peer Reviewed & Refereed Journal |

|| Volume 13, Issue 5, May 2024 ||

| DOI:10.15680/IJIRSET.2024.1305357 |

power filter (SAPF) approaches. Shunt active power filters are used to compensate for reactive and harmonic currents that are drawn by non-linear loads. This will remove harmonics and produce a sinusoidal supply current. MATLAB/Simulink is utilized to execute harmonic mitigation on Tawor Ceramic Ceramics Company, Hawassa, Ethiopia, with the goal of reducing the total harmonic distortion (THD) to a level that complies with IEEE standards.

L. MihetPopa, R. Bayindir, F. Blaabjerg, S. Vadi, and S. Padmanaban Microgrids, which are networks of distribution systems made up of dispersed energy sources like wind and solar turbines, are among the most widely used energy sources. In addition, microgrids comprise energy storage devices and loads (including commercial and residential ones) that may function in both islanded and grid-connected modes. For dispersed renewable energy sources connected to the current grid, microgrids are an effective source of low-cost, clean, and renewable energy; nevertheless, because of the features of these renewable energy sources, the microgrid also faces several challenges. Voltage collapses, voltage and frequency variations, and phase difference failures in both islanded mode and grid-connected mode operations are the principal causes of these challenges. In order to remove the aforementioned issues that have an impact on power quality, intelligent optimization techniques must be used to provide transient stability to the microgrid structure. In order to achieve transient stability in the islanded or grid-connected mode operations of a microgrid made up of renewable energy sources, this study proposes optimization and control strategies. The outcomes of these strategies were contrasted, and the benefits and drawbacks of the numerous approaches put forward were discovered by reviewing research in the literature. In order to identify and direct future research, a thorough assessment of the literature on microgrid stability is offered.

R. K. Ghadai, N. Priyadarshi, S. Padmanaban, A. R. Panda, and R. Patel. Selected proceedings of the international conference ETAEERE 2020 are included in this book, which addresses current problems with energy efficiency and management in the context of power systems. AGC in two area hydro thermal power system, energy-efficient and dependable depth-based routing protocol for underwater wireless sensor network, power line communication, cost optimization of a ring frame unit in the textile industry, rectenna for RF energy harvesting, ecological and energy dimension in infrastructural designs, and modeling, simulation, and optimization-based research are among the subjects covered in the material. This book can be useful for scholars, industry experts, and students.

According to E. Sundaram and M. Venugopal, shunt active power filters are frequently employed to get rid of current harmonics that are produced on the source side when non-linear loads are present. To reduce supply current harmonics and provide non-linear loads with the necessary reactive power, this design comprises of a DC capacitor acting as a shunt active power filter and a three phase, three level diode clamped multilevel inverter. This study presents the implementation of a three phase, three level SAPF on an embedded platform utilizing synchronous reference frame method. Reference signals are converted from an a-b-c stationary frame to a 0-d-q rotating frame in SRF theory. Using a PI controller, the reference signals in the 0–d–q rotating frame are adjusted to provide the required reference signals. The measured amplitudes of the reference phase voltages are directly used to compute the PWM signal generation for the three phases, three level inverter. With the help of the Xilinx XC3SD1800A – FG676-4 Spartan 3A DSP FPGA controller, the SAPF is implemented practically. To verify the efficacy of the suggested system, a prototype hardware model is compared with the simulation results obtained via MATLAB/SIMULINK simulation of this system. According to the IEEE-519 standard, it is straightforward to apply the SAPF to reduce total harmonic distortion below 5% based on the results of the research.

This article by A. Raj, S. R. Arya, and J. Gupta describes a low power solar PV array system that is fed by a DC–DC converter. For this PV array system, a solar panel with a single diode is built and modeled. The mechanism will function more accurately when the solar panel's irradiation is low. The same system uses the Maximum Power Point Tracking (MPPT) control algorithm in order to achieve more efficiency. The characteristics curves for the solar panel's current v/s voltage (I–V) and power v/s voltage (P–V) are derived using MATLAB simulation. The curves derived from the experiment data are also compared to the simulation curves. A thorough analysis of solar-fed DC–DC converters using the soft-switching approach is also carried out. This soft-switching method is created with the use of capacitors and resonant inductors. The circuit switching losses are minimized by these passive parts. To remove the switching losses that are created in the circuit during switching transitions, employ the Zero Voltage Switching (ZVS) approach. This method also lessens the noise caused by the discharge of junction capacity. This proposed ZETA and SEPIC converter-based system is modeled and simulated using a MATLAB software, and its efficiency and losses are measured through experiments. In comparison to its traditional ZETA and SEPIC converter, the performance study of ZVS ZETA and SEPIC converter yielded efficiency gains of 1.97% and 7.23% under Perturb and Observe MPPT control and 4.14% and 0.41% under Incremental Conductance MPPT control, respectively.

|e-ISSN: 2319-8753, p-ISSN: 2347-6710| www.ijirset.com | Impact Factor: 8.423| A Monthly Peer Reviewed & Refereed Journal |

|| Volume 13, Issue 5, May 2024 ||

| DOI:10.15680/IJIRSET.2024.1305357 |

II. GRID CONNECTED NETWORKS

2.1 Introduction

Microgrid systems are decentralized networks of energy sources, storage systems, and loads that can operate independently or in connection with the main power grid. They provide resilience, reliability, and flexibility to the energy infrastructure, allowing for efficient integration of renewable energy sources and improved energy management

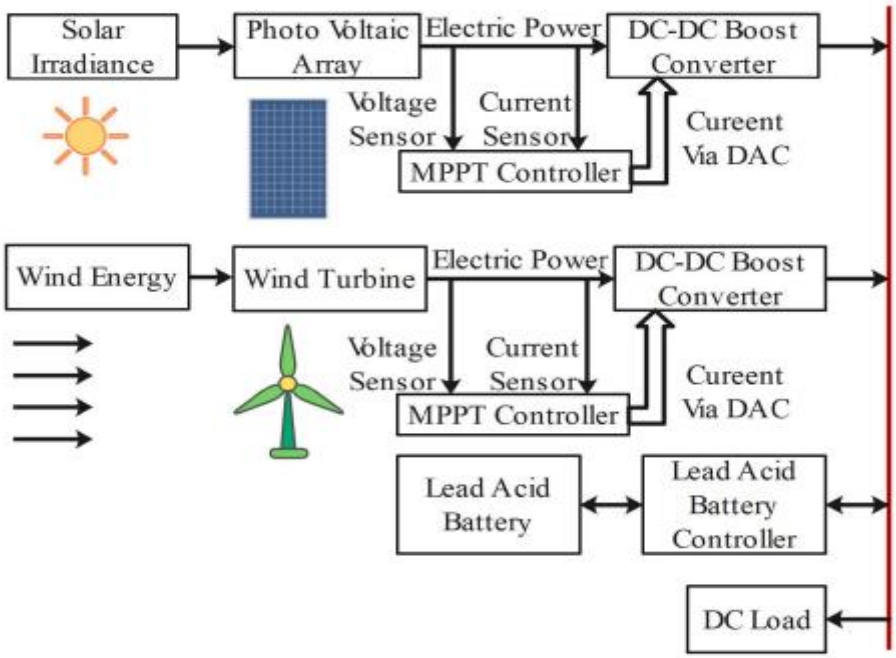

Figure 1. Structure of general microgrid system.

Parameter Variable	Ratings
Input Voltage Range DC (Min)	150V
O/P voltage range DC (Max)	350V
Switching Frequency up to	100KHz
Inductor (L)	5mH
Capacitors (C)	1500uF
IGBT	1200V/100A

Table 1. DC-DC boost converter specifications.

|e-ISSN: 2319-8753, p-ISSN: 2347-6710| www.ijirset.com | Impact Factor: 8.423| A Monthly Peer Reviewed & Refereed Journal |

|| Volume 13, Issue 5, May 2024 ||

| DOI:10.15680/IJIRSET.2024.1305357 |

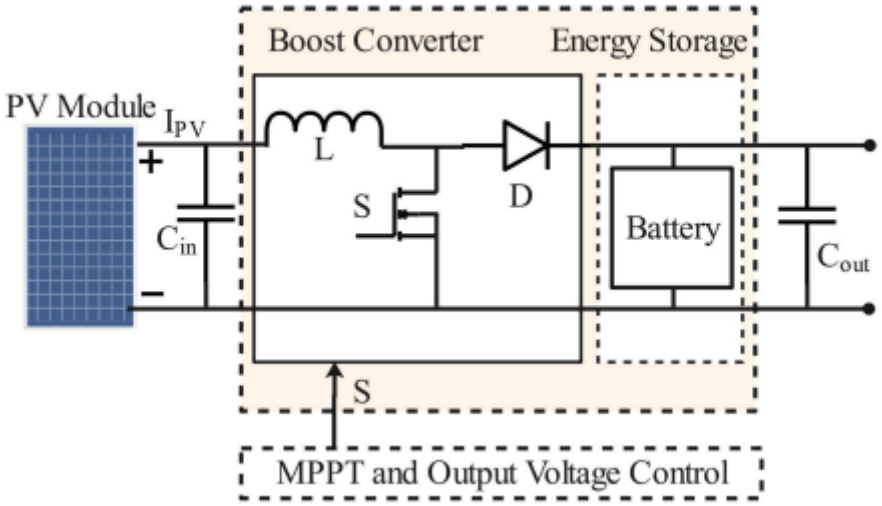

Figure 2. PV system with power converter

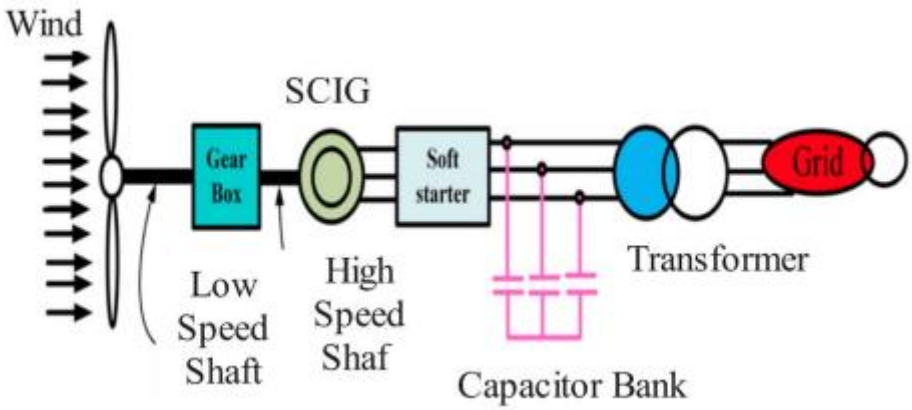

Figure 3. Basic diagram of SCIG wind turbine

A block schematic of a typical micro grid system is shown in Fig. 1. A hybrid of wind and solar systems is called a microgrid. In addition, a bidirectional battery bank was employed to raise the power system's dependability. In this instance, the PV, wind, and battery systems are connected at the DC bus. An inverter is used to connect these systems to the grid system. Maintaining synchronization between the hybrid system and the grid is the aim of this inverter [13]. The various loads were run on the suggested hybrid system.

Parameter Variable	Ratings
DC Link capacitor (CDC)	220 pF
DC Link voltage	640 V
Carrier Frequency	2.08 KHz

Table 2. Specifications

|e-ISSN: 2319-8753, p-ISSN: 2347-6710| www.ijirset.com | Impact Factor: 8.423| A Monthly Peer Reviewed & Refereed Journal |

|| Volume 13, Issue 5, May 2024 ||

| DOI:10.15680/IJIRSET.2024.1305357 |

2.2 PV Solar System

Out of all the disrupted energy sources, the solar energy system has played a significant part in the history of renewable energy due of its affordability, dependability, and availability in the natural world. Photons from the sun's irradiance are converted into electrical energy via solar cells. With the aid of an analogous electric circuit, electric current that first passes from solar cells is subsequently transformed into PV voltage [14]. Temperature and sun irradiation both affect the resulting DC voltage. As seen in Fig. 2, an MPPT based DC-DC boost converter is suggested as a means of obtaining a constant DC voltage from the solar system. Tracking the solar power's maximum output is the MPPT's goal [15]. To achieve the necessary voltage and current ratings, these cells were set up in series and parallel. The boost converter's specifications shown in Table 1. Monitoring a PV system's instantaneous power is the foundation of MPPT. PV voltage and current were used to compute PV power. A P&O MPPT is suggested for this system [16]. The reference signals are controlled by means of voltage and current controllers. These reference signals are utilized to create the duty cycle needed for the DC-DC converter using a traditional PWM controller [17].

2.3 WIND Energy System

Another important component of this unstable energy system is wind turbines. When wind is present in the environment, energy is converted into two forms: mechanical energy via the use of turbine blades, and electrical energy through the use of an electrical generator [18]. The wind turbine additionally includes a gearbox system to change a low-speed shaft into a high-speed shaft in addition to these parts [19]. To increase dependability, a pitch angle controller was also used to spin the wind blades in accordance with the wind's direction [20]. A wind vane was used to gauge the wind's speed as it approached the wind turbine. Fig. 3 depicts the general wind turbine system structure using a conventional generator. The power produced by the wind turbine system is the mathematical representation of the wind energy system, as stated in (1).

$$\boldsymbol{P_{mech} = \frac{1}{2} C_p\,(\lambda, \beta) m A \rho V^3}$$

Induction and synchronous generators are the two types of generators currently on the market [21]. In this instance, the wind turbine produced electricity through the use of a squirrel-type induction generator [22]. Synchronization with the AC grid was accomplished through the use of an AC-DC-AC converter.

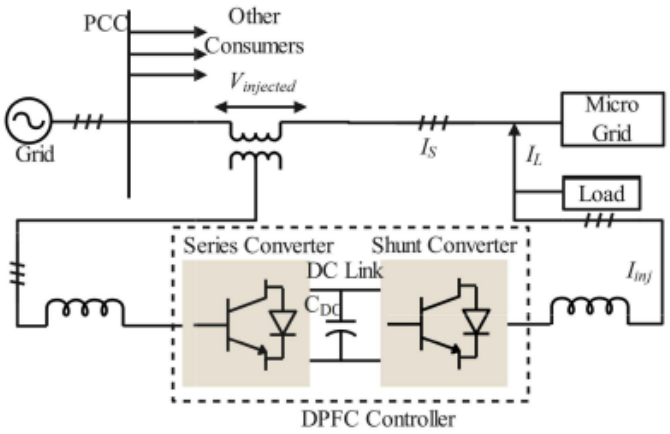

Figure 4. Proposed DPFC controller block diagram

2.4 Perturb and Observer MPPT Algorithm

Problems with optimization are common in many branches of science and technology. Due to the actual and practical nature of the objective function or model constraints, these problems can occasionally be extremely complex [23]. An objective function subject to intricate and nonlinear characteristics with strict equality and/or equality constraints is typically minimized or maximized in an optimization problem. Under the perturb and observe technique, the output power is measured after the system monitors changes in the array voltage [24]. Fig. 4 displays a flowchart of the P&O MPPT algorithm. This flowchart measures the PV panel's voltage and current and computes the PV power [25]. Instantaneous PV power was used to measure the obtained PV power. The necessary reference current signal is measured based on these findings. This cycle was continually repeated. This P&O technique's primary drawback is its inability to adapt to ongoing changes in environmental factors like sunlight and irradiance. To get a better output, the output is constantly compared to the previous output. Because of its complexity, optimization algorithms are a good fit

|e-ISSN: 2319-8753, p-ISSN: 2347-6710| www.ijirset.com | Impact Factor: 8.423| A Monthly Peer Reviewed & Refereed Journal |

|| Volume 13, Issue 5, May 2024 ||

| DOI:10.15680/IJIRSET.2024.1305357 |

for solving the controller design [26]. The field of electronic design through optimization algorithms is well-established and has the potential to offer an ideal solution for designs with high levels of complexity. The MPPT algorithm (perturb and observe) in this study explains how the solar panels track their maximum power.

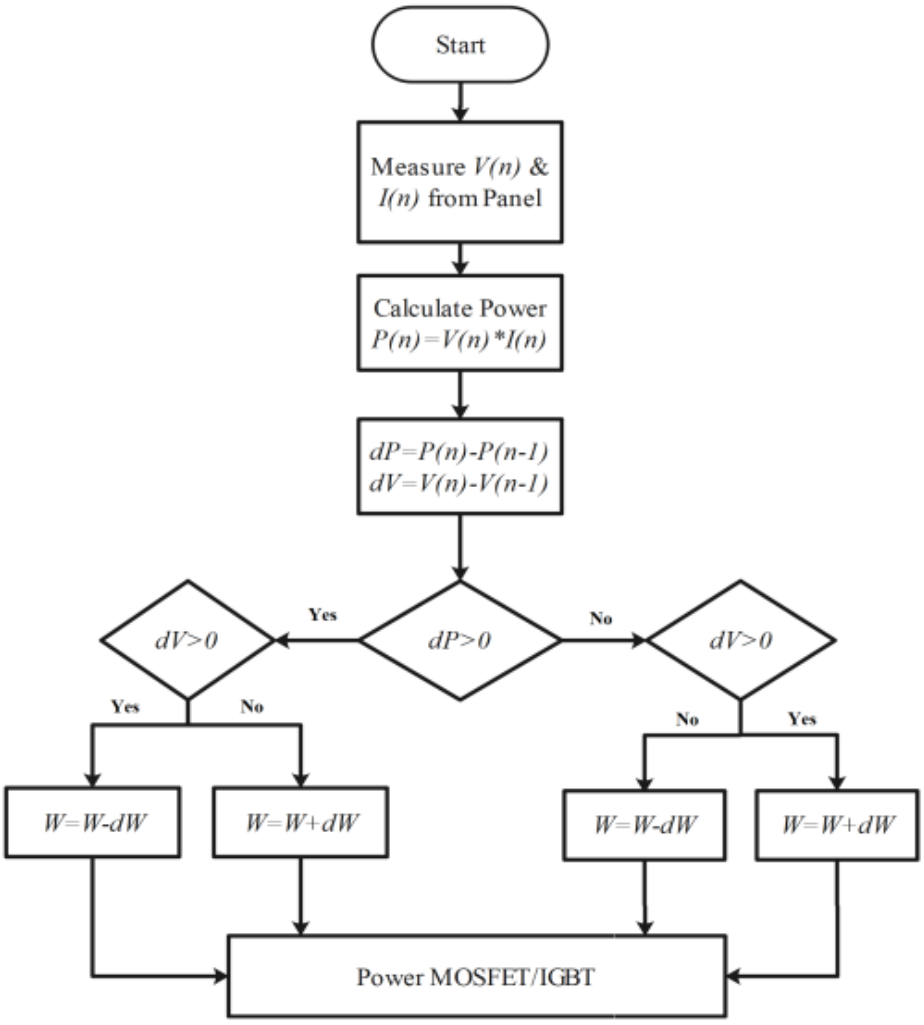

Figure 5. Flowchart representation of P&O technique

2.5 Inverter Control Diagram

One tool for improving power quality is the distributed power flow controller (DPFC). As seen in Fig. 5, it is composed of an a-shunt converter and a two-converter series converter. For the load and microgrid, voltage harmonic compensation is achieved through a series converter, while current harmonic compensation is achieved through a shunt converter [27]. The current controllers in a double loop served as the basis for the design of this inverter control diagram. In this instance, the system's transient stability is enhanced by the inner loop while the steady-state error of the current comparator is regulated by the outer loop, also known as proportional resonant controllers [28]. Fig. 6 displays the converter control diagram. The load, system voltage, and current were measured in this controller. Using Park's method [29], these load currents were transformed into a d-q transformation. The load, loss, and hybrid system power are used to calculate the grid's active power. (2) was used to calculate the grid power.

$$P_g = P_L + P_{SL} - P_{PV} \quad (2)$$

|e-ISSN: 2319-8753, p-ISSN: 2347-6710| www.ijirset.com | Impact Factor: 8.423| A Monthly Peer Reviewed & Refereed Journal |

|| Volume 13, Issue 5, May 2024 ||

| DOI:10.15680/IJIRSET.2024.1305357 |

The reference current signal ($i * s_1$) is identified and applied to an inner current controller based on this computed power. To create the gate signals needed for the inverter, the inner loop of the reference current is applied to the hysteresis loop and contrasted with the supply current. Table 2 contains the DPFC's specifications.

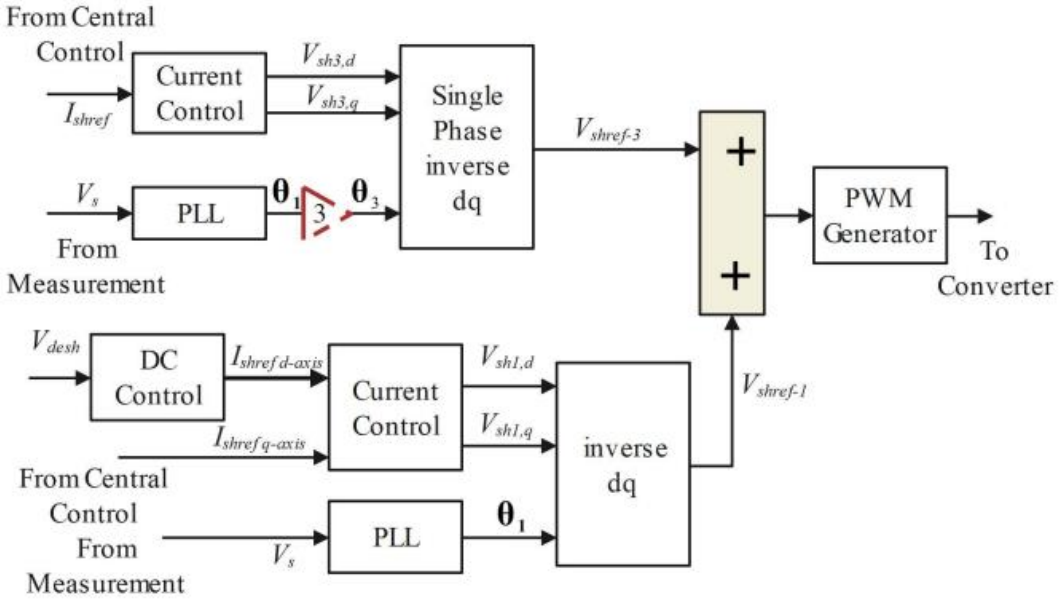

Figure 6. Proposed DPFC control diagram

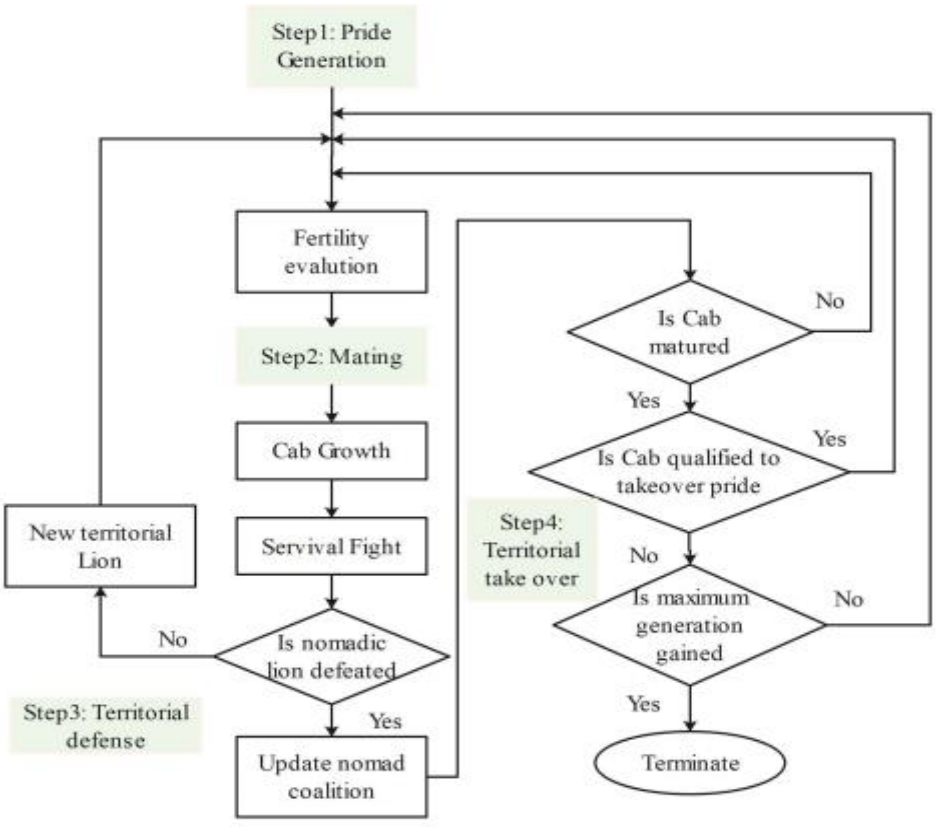

Figure 7. The flow structure of the proposed LOA based DPFC

|e-ISSN: 2319-8753, p-ISSN: 2347-6710| www.ijirset.com | Impact Factor: 8.423| A Monthly Peer Reviewed & Refereed Journal |

|| Volume 13, Issue 5, May 2024 ||

| DOI:10.15680/IJIRSET.2024.1305357 |

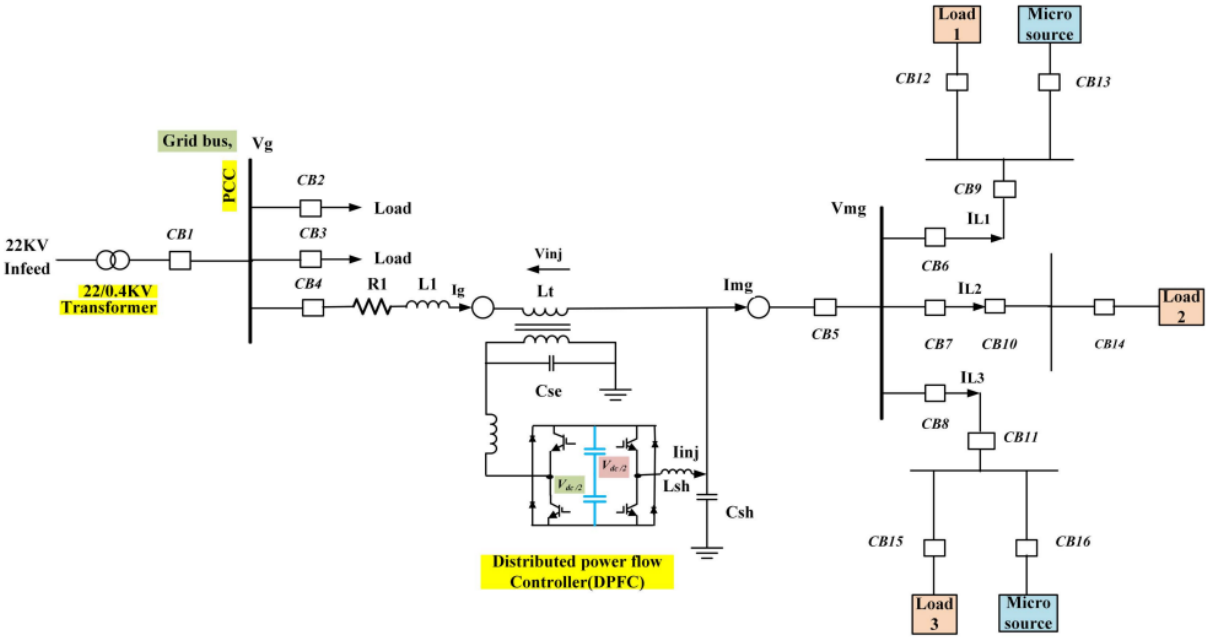

Figure 8. The proposed system in MATLAB/Simulink

Parameter Variable	Ratings
Maximum Power	100W
Voltage at max Power	18.7V
Current at max Power	5.35A
Open Circuit Voltage	22.32V
Short Circuit Current	5.65A
No. of panels	10
No. of strings	I
Type of Cell	Polycrystalline Silicone

Table 3. System Parameters for PV System

Parameter Variable	Ratings
Rated power output (W)	5000
Peak power output (W)	6800
Rated Voltage	415
Cut-in- Speed (m/s)	2
Nominal wind speed (m/s)	8
Cut-out- Speed (m/s)	18
Rated Rotor Speed (RPM)	250
Generator Efficiency	0.95
Noise Level	<30db
Number of Blades	3
Rotor diameter (mm)	3600

|e-ISSN: 2319-8753, p-ISSN: 2347-6710| www.ijirset.com | Impact Factor: 8.423| A Monthly Peer Reviewed & Refereed Journal |

|| Volume 13, Issue 5, May 2024 ||

| DOI:10.15680/IJIRSET.2024.1305357 |

Blade Material	Glass fiber
Generator Type	SCIG
Cp value at max	0.18

Table 4. Specifications of wind turbine

2.6 Fuzzy Logic Controller

A sophisticated mathematical technique called fuzzy logic enables the resolution of challenging simulated problems with numerous input and output variables. Given that fuzzy logic can produce recommendations for a particular output state interval, it is imperative that this mathematical technique be clearly separated from more widely used logics like Boolean algebra. The basic ideas of fuzzy logic are summarized in this paper.

A mathematical system that solely relies on digital logic is called a fuzzy control system. Four steps make up the controlling process in fuzzy logic: a) membership function, b) fuzzification, c) rule-based formation, and d) defuzzification [30]. Fuzzification is the process of converting analog input into fuzzy sets and expressing the input and output graphically under the membership function (triangular membership function, for example). A rule-based formation can be used to express the relationship between the input and output [31]. Here, an if-then statement is used to express the rules, as seen in Fig. 7. The number of memberships in the fuzzy logic inputs, which are connected to digital operators (AND or OR), determines how many rules are created. Through the defuzzification process, the output from the fuzzy set is expressed as a crisp value. The centroid was selected as the defuzzification technique in this instance [32].

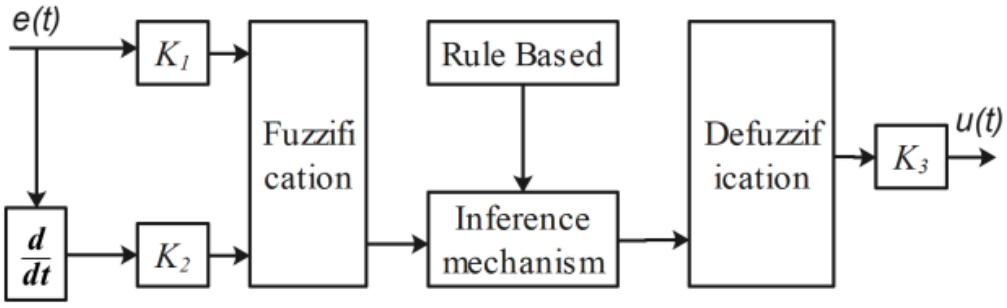

Figure 9. Fuzzy Logic based DPFC block diagram

These days, stochastic models, models derived from mathematical logic, or models that obey the laws of physics are typically used to characterize control systems. One common challenge with these built models is figuring out how to transform a given problem into an appropriate mathematical model. It is certainly made possible by the sophisticated computer technology of today, but maintaining such systems is still too difficult.

By including a tolerance margin for a suitable degree of imprecision, vagueness, and uncertainty during the modeling phase, these complex systems can be made simpler. Consequently, no system is perfect from the start, but for the most part, it can solve the issue in a way that is appropriate. In knowledge-based systems, it has already been found that even missing input data can produce satisfactory results. By enabling the sensible use of imperfect information, fuzzy logic reduces complexity. It can be put into practice using software, hardware, or a combination of the two. Stated differently, the fuzzy logic approach to problem solving simulates human decision-making processes, albeit at a significantly faster pace.

The methods of fuzzy logic analysis and control depicted in Figure 1 can be characterized as follows:

1. Getting one or more measurements, or an evaluation of the state of affairs in a system that will be examined or managed.
2. Using conventional non-fuzzy processing in conjunction with human-based, fuzzy "if-then" rules that can be articulated in plain language to process all incoming inputs.
3. Weighing and averaging the outcomes of each individual rule to create a single output signal or decision that controls or directs a controlled system. The output signal that results is an exact defuzzified value.

|e-ISSN: 2319-8753, p-ISSN: 2347-6710| www.ijirset.com | Impact Factor: 8.423| A Monthly Peer Reviewed & Refereed Journal |

|| Volume 13, Issue 5, May 2024 ||

| DOI:10.15680/IJIRSET.2024.1305357 |

Below is diagram for Fuzzy Logic Control/Analysis Method.

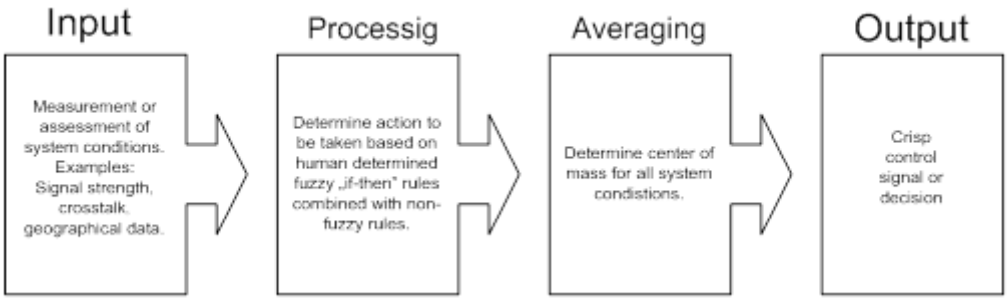

Figure 10. The fuzzy logic Control-Analysis method

Fuzzy logic requires descriptions or numbers to be represented in order to function. For instance, the speed can be described as "slow" or as the value 5 m/s. When used by different people, the term "slow" can have different meanings, so it's important to interpret it in light of the surrounding circumstances. Certain values are simple to categorize, while others may be more challenging due to the limitations of human comprehension in various contexts. When describing the same speed, one person may say it's "slow," while another may say it's "not fast." So-called fuzzy sets can be used to help distinguish between these differences.

The four main components shown in Figure 2 are typically used to create a fuzzy logic control system: the defuzzification interface, fuzzy inference engine, fuzzy rule matrix, and fuzzification interface. We'll go into more detail about each component and the fundamental fuzzy logic operations below.

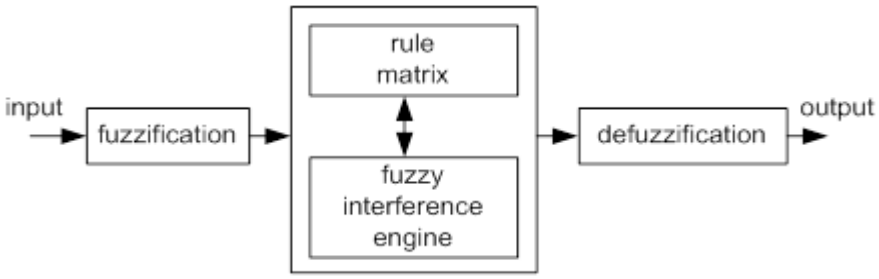

Figure 11. Fuzzy logic controller

2.7 Fuzzy Logic Basic Operations

A thorough theory of fuzzy logic can be found in [2], but below is some basic information about the subject.

• The Universe of Discourse refers to the entire range of values that can be regarded as fuzzy input for a system.

• Fuzzy Set: A fuzzy set (μ) is a function that maps the unit interval to the reference set X.

$$\mu: X \rightarrow [0,1] \quad (2)$$

μ(X) represents the set of all fuzzy sets of X.

• Membership Function: It is a graphical representation of fuzzy sets, μF(x).

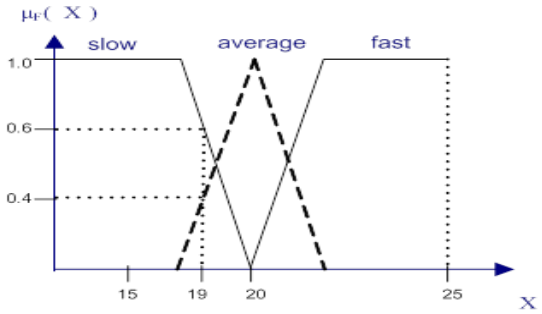

Figure 12. An example of fuzzy logic membership function

|e-ISSN: 2319-8753, p-ISSN: 2347-6710| www.ijirset.com | Impact Factor: 8.423| A Monthly Peer Reviewed & Refereed Journal |

|| Volume 13, Issue 5, May 2024 ||

| DOI:10.15680/IJIRSET.2024.1305357 |

For a fuzzy variable called velocity, Figure 3 displays the membership functions of three fuzzy sets: "slow," "average," and "fast." All potential Velocity values are created by the discourse universe, i.e., X = 19. The membership value of the fuzzy set "slow" is 0.6 for a velocity value of 19 km/h. μslow (19) = 0.6 as a result. Likewise, $\mu_{fast}(19) = 0$ and μaverage(19) = 0.4.
Assistance: The crisp set of all points in the Universe of Discourse U such that the membership function of F does not equal zero is the support of a fuzzy set F.

$$\mu_F(u) > 0 \qquad (2)$$

Crossover point: An element in U with a membership function of 0.5 is this one.
Center: The point (or points) at which μF(u) reaches its maximum value is the center of a fuzzy set F.

2.8 Fuzzification Method
Providing input parameters for the given fuzzy system—which will be used to calculate the output result—is the first step in the fuzzy logic process. Pre-defined input membership functions—which can take on various forms—are used to fuzzify these parameters. The most popular shapes are triangles, though bell, trapezoidal, sinusoidal, and exponential shapes can also be employed. Simpler functions won't overload the implementation or require sophisticated computing. By positioning a selected input variable on the horizontal axis and quantifying the input variable's grade of membership on the vertical axis, one can determine the degree of membership function. A membership function only needs to vary between zero and one. That is all. When an input variable has a value of one, it fully belongs to the fuzzy set, whereas when it has a value of zero, it does not belong to the fuzzy set.

There is a distinct membership function linked to each input parameter. The membership functions link the effective rules and the values of each input to a weighting factor. Each active rule's degree of influence or degree of membership (DOM) is determined by these weighting factors. A set of fuzzy output response magnitudes is generated by multiplying the membership weights for each active rule by their logical product. Combining and defuzzifying these output responses is the only thing left to do.

2.9 Rule Matrix
A rule matrix that resembles fuzzy logic schemes. The relationships between the control output and the input variables (such as error and rate of change of error) are defined in this table.

2.9.1 Fuzzy rules table
Fuzzy sets and fuzzy operators in the form of conditional statements are described by the rule matrix. This could be one fuzzy if-then rule. If x = A, then y = Z, where Z is a set of definable consequences and A is a set of requirements that must be met.

Fuzzy operators are used in rules with multiple parts to combine multiple inputs: AND = min, OR = max, and NOT = additive complement. Figure 13 displays a geometrical demonstration of fuzzy operators.

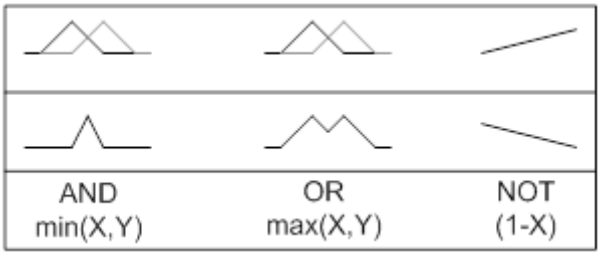

Figure 13. Graphical interpretation of fuzzy operators

A straightforward graphical tool for mapping the fuzzy logic control system rules is the rule matrix. It accepts two or more input variables and outputs one response variable as the logical product of those variables (AND or OR). The maximum and minimum values for the degree of previous rule can be used to determine the degree of membership for the rule matrix output. It is frequently likely that we will receive multiple values for the degree of membership following the assessment of all applicable rules for the input. In this instance, the simulation must account for the minimum, maximum, and average membership degrees, among the three possibilities.

|e-ISSN: 2319-8753, p-ISSN: 2347-6710| www.ijirset.com | Impact Factor: 8.423| A Monthly Peer Reviewed & Refereed Journal |

|| Volume 13, Issue 5, May 2024 ||

| DOI:10.15680/IJIRSET.2024.1305357 |

2.9.2 Inference Mechanisms

Fuzzy logic can be used to map a given input to an output through the inference mechanism. It makes use of all the components logical operations, if-then rules, and membership functions—that were covered in earlier sections. Mamdani and Sugeno inference systems are the two most popular varieties. Their approaches to figuring out outputs differ.

2.9.3 Mamdani method

The examples that follow are predicated on two fuzzy control rules, represented as

- R1: Z is C1 if x is A1 and y is B1.
- R2: z is C2 if x is A2 and y is B2.

Z equals C as a result, with x equaling x0 and y equaling y0.

The rules' firing levels, represented by αi for i = 1 and 2, are computed using,

$$\alpha_1 = A_1(x_0) \wedge B_1(y_0) \quad (3)$$

$$\alpha_2 = A_2(x_0) \wedge B_2(y_0) \quad (4)$$

The individual rule outputs are derived by

$$C_1'(\omega) = \left(\alpha_1 \wedge C_1(\omega)\right) \quad (5)$$

$$C_2'(\omega) = (\alpha_2 \wedge C_2(\omega)) \quad (6)$$

Then the overall system output is calculated by comparing the individual rule outputs

$$C(\omega) = C_1'(\omega) \vee C_2'(\omega) = \left(\alpha_1 \wedge C_1(\omega)\right) \vee \left(\alpha_2 \wedge C_2(\omega)\right) \quad (7)$$

In order to achieve a deterministic control action, the selected defuzzification mechanism needs to be put into practice.

2.9.4 Sugeno method

The following examples are based on two fuzzy control rules in the format of

- R1: z is z1 = a1x1+b1y1 if x is A1 and y is B1.
- R2: z is z2 = a2x2+b2y2 if x is A2 and y is B2.
- The outcome is z0, where x = x0 and y = y0.

Using equations (3) and (4), the firing levels of the rule are determined in the same manner as in the Mamdani method. The relationships listed below are used to calculate the individual rule outputs.

$$Z_1 = a_1 \cdot x_0 + b_1 \cdot y_0 \quad (8)$$

$$Z_2 = a_2 \cdot x_0 + b_2 \cdot y_0 \quad (9)$$

If there are n rules in the rule matrix, the crisp control result derived from the following equations

$$Z_0 = na_i z_i \quad (10)$$

where i = 1, .., n, and αi is a firing level of the i rule.

The Sugeno method is computationally efficient and thus works well with linear techniques. Adaptive and optimization techniques are appropriate. Moreover, it ensures output surface continuity and is well-suited for mathematical analysis. The Mamdani method has the advantage of being widely accepted and intuitive. It may work well with human input.

2.9.5 Defuzzification Mechanisms

Finding a single, distinct value that encapsulates the fuzzy set is the defuzzification task. The following mathematical methods are available: weighted average, maximum, maximum, bisector, centroid, and mean. Figure 5 shows an example of how the values for each method are selected.

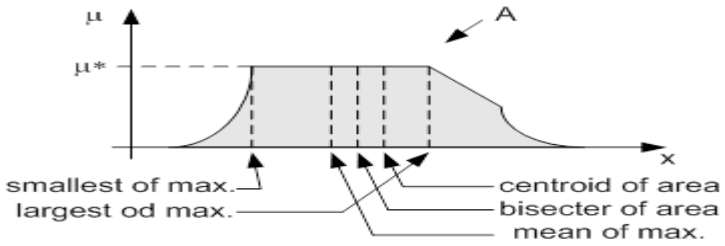

Figure 14. Graphical demonstration of defuzzification methods

|e-ISSN: 2319-8753, p-ISSN: 2347-6710| www.ijirset.com | Impact Factor: 8.423| A Monthly Peer Reviewed & Refereed Journal |

|| Volume 13, Issue 5, May 2024 ||

| DOI:10.15680/IJIRSET.2024.1305357 |

The most popular approach is centroid defuzzification because of its high accuracy. It offers the membership function's center of the area under the curve. It places heavy computational demands on membership functions that are complex. It can be stated using the formula that follows.

$$Z_0 = \frac{\int \mu_i(x)\, x\ dx}{\int \mu_i(x)\, dx} \quad (11)$$

where X is the output variable, u_i is a membership function, and Z_0 is the defuzzified output.
A vertical line that splits the area under the curve into two equal sections is used in bisector defuzzification.

$$\int_{\alpha}^{z} \mu_A(x)\, dx = \int_{z}^{ß} \mu_A(x)\, dx \quad (12)$$

The average value of the total outputs from the membership function is used in the mean of maximum defuzzification method.

$$Z_0 = \frac{\int_{x'} dx}{\int_{x'} dx'} \quad (13)$$

Where x' = {x; μA(x) = μ*}.
The minimum value of the combined membership function outputs is used in the smallest of maximum defuzzification methods.

$$Z_0 \in \{x|\mu(x) = min\ \mu(\omega)\}\text{ssss} \quad (14)$$

Largest of maximum defuzzification method uses the maximum value of the aggregated membership function outputs.

$$Z_0 \in \{x|\mu(x) = \max \mu(\omega)\} \quad (15)$$

The weighted sum of these peak values is determined by the weighted average defuzzification method, which is based on the peak value of each fuzzy set [4]. The following formula determines the crisp value of output based on these weight values and the degree of membership for fuzzy output.

$$Z_0 = \frac{\sum \mu(x)_i \times W_i}{\sum \mu(x)_i} \quad (16)$$

Where Wi and is the output singleton's fuzzy output weight value, and μi is the output singleton's degree of membership.

2.10 Basic Controller Types
Three fundamental behavior types or modes are used by PID controllers: D is derivative, 'I' is integrative, and 'P' is proportional. In control systems, a derivative mode is rarely employed alone, despite the fact that proportional and integrative modes are also frequently employed as single control modes.
In practical systems, combinations like PI and PD control are frequently used.

2.10.1 P Controller
In general, it can be said that P controller cannot stabilize higher order processes.
For the 1st order processes, meaning the processes with one energy storage, a large increase in gain can be tolerated. Proportional controller can stabilize only 1st order unstable process. Changing controller gain K can change closed loop dynamics. A large controller gain will result in control system with:
a) Smaller steady state error, i.e. better reference following
b) Faster dynamics, i.e. broader signal frequency band of the closed loop system and larger sensitivity with respect to measuring noise
c) smaller amplitude and phase margin

|e-ISSN: 2319-8753, p-ISSN: 2347-6710| www.ijirset.com | Impact Factor: 8.423| A Monthly Peer Reviewed & Refereed Journal |

|| Volume 13, Issue 5, May 2024 ||

| DOI:10.15680/IJIRSET.2024.1305357 |

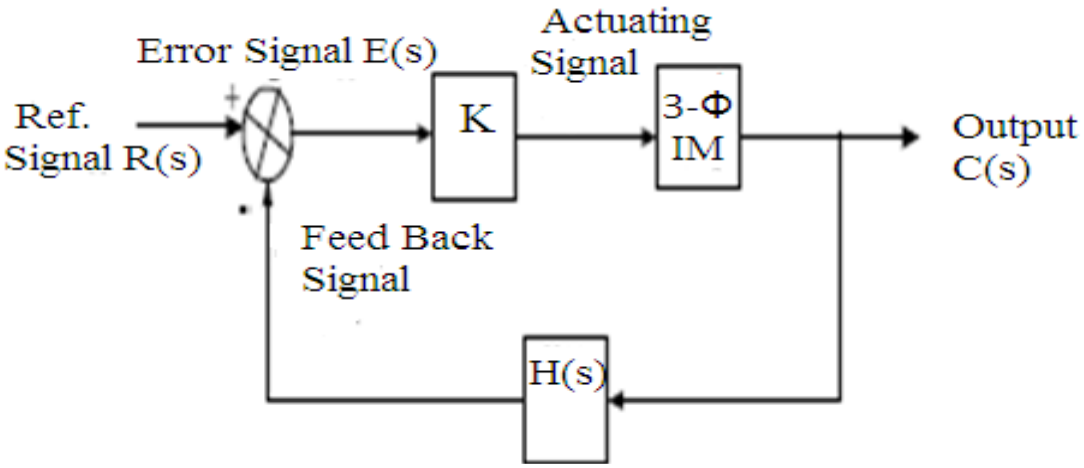

Figure 15.Block diagram of P controller

The error of signal given as follows: $e(t) = k[r(t) - h(t)]$
A high gain is required when using a P controller to reduce steady state error. Large gains are used with no problems in stable systems. One energy storage unit makes up these systems (1st order capacitive systems). P controllers can be used with such processes if constant steady state error can be tolerated. If the sensor produces a measured value with error or if the measured value is not very important in any case, small steady state errors can be tolerated.

2.10.2 PD Controller
When error prediction can enhance control or when system stabilization is required, D mode is employed. It is evident from the D element's frequency characteristic that it has a 90° phase lead. Derivatives are frequently taken from the system output variable rather than the error signal. This is done to prevent the effects of a sudden change in the reference input, which could result in a sudden change in the error signal's value. The control output will abruptly change in response to a sudden change in the error signal. It is appropriate to design D mode to be proportionate to the change in the output variable in order to prevent that.

PD controllers are frequently used to control moving objects, including ships, rockets, flying and underwater vehicles, etc. One of the causes is the PD controller's stabilizing effect on abrupt changes in the heading variable y(t). A "rate gyro" is frequently used as a heading change sensor for moving objects in order to measure their velocity.

2.10.3 PI Controller:
Forced oscillations and steady state errors will be eliminated by the PI controller, enabling the P and on-off controllers to operate, respectively. However, the system's overall stability and response speed are negatively impacted by the introduction of integral mode.

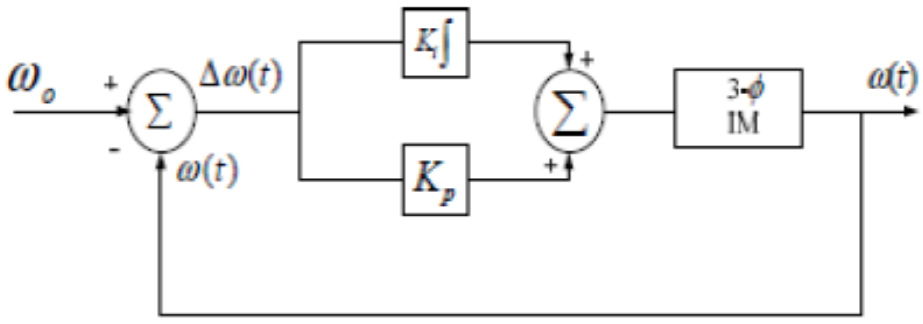

Figure 16. Block diagram of PI controller

In this instance, the controller output is: $u(t) = K_p e(t) + K_i \int e(t)\,dt$.

|e-ISSN: 2319-8753, p-ISSN: 2347-6710| www.ijirset.com | Impact Factor: 8.423| A Monthly Peer Reviewed & Refereed Journal |

|| Volume 13, Issue 5, May 2024 ||

| DOI:10.15680/IJIRSET.2024.1305357 |

As a result, the PI controller won't quicken response time. It makes sense because the PI controller lacks the ability to forecast the error's future course. This issue can be resolved by using the derivative mode, which can reduce the controller's reaction time by predicting what will happen to the error in the near future.

In industry, PI controllers are widely used, particularly when response time is not a concern. When using a control without a D mode:

- Fast response of the system is not required
- Large disturbances and noise are present during operation of the process
- There is only one energy storage in process (capacitive or inductive)
- There are large transport delays in the system

2.10.4 PID Controller

The PID controller contains all of the essential dynamics: a quick reaction to changes in the controller input (D mode), an increase in control signal to drive error towards zero (I mode), and appropriate action inside the control error area to remove oscillations (P mode). Derivative mode enhances system stability and allows for an increase in gain K and a drop-in integral time constant Ti, resulting in a faster controller response.

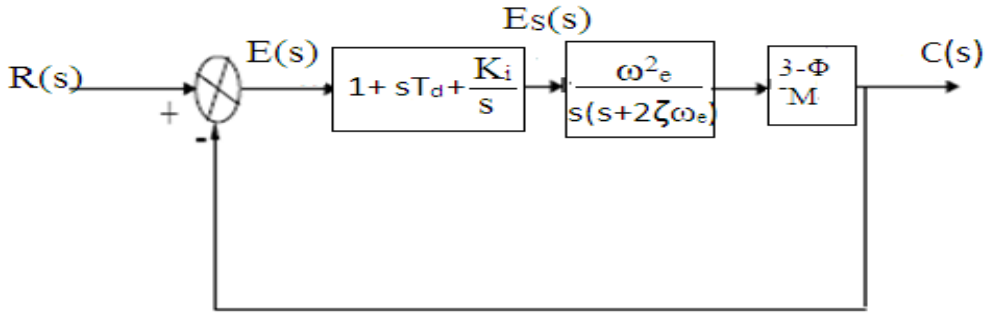

Figure 17. Block diagram of PID controller

Controller output is,

$$u(t) = K_p e(t) + K_i \int e\,(t)\,dt + K_d \frac{de(t)}{dt}$$

PID controllers are utilized when dealing with higher order capacitive systems (processes with more than one energy store) whose dynamics differ from those of an integrator (as in many thermal processes). PID controllers are commonly employed in industry, but they may also be utilized to control mobile objects (including course and trajectory following) where stability and exact reference tracking are necessary. Most conventional autopilots use PID controls.

Table 5. Effects of Coefficients

2.11 Converter

Parameter	Speed of response	Stability	Accuracy
increasing K	increases	deteriorate	improves
increasing Ki	decreases	deteriorate	improves
increasing Kd	increases	improves	no impact

|e-ISSN: 2319-8753, p-ISSN: 2347-6710| www.ijirset.com | Impact Factor: 8.423| A Monthly Peer Reviewed & Refereed Journal |

|| Volume 13, Issue 5, May 2024 ||

| DOI:10.15680/IJIRSET.2024.1305357 |

2.11.1 Introduction

The term "converters" refers to a system that converts one type of electrical energy to another. For instance, AC to DC or DC to AC. In this context, converting ac to dc is referred to as "rectification," whereas converting dc to ac is referred to as "inversion."

Power conversion systems can be classed by the kind of input and output power.

- AC to DC (rectifier)
- DC to AC (inverter)
- DC to DC (DC-to-DC converter)
- AC to AC (AC-to-AC converter)
- AC to DC converters (Diode bridge rectifier)
- A diode rectifier circuit converts ac input voltage into a fixed dc voltage. The input voltage may be single phase or three-phase.
- AC to DC converters (phase-controlled rectifiers)

These circuits convert constant ac voltage to variable dc output voltage. These Rectifiers commutate with line voltage. These are utilized in synchronous machinery, chemical industries, and direct current drives. Phase regulated converters can be supplied from both single and three-phase sources.

Parameter	Rise Time	Overshoot	Time	S.S Error	Stability
Kp	Decrease	Increase	Small Change	Decrease	Worse
Ki	Decrease	Increase	Increase	Significant Decrease	Worse
Kd	Minor Dec.	Minor Dec.	Minor Dec.	No change	If Kd small, Better.

2.11.2 DC to AC converters (inverter)

A DC to AC converter generates an AC output waveform from a DC source. Applications include adjustable speed drives (ASD), uninterruptible power supply (UPS), flexible AC transmission systems (FACTS), voltage compensators, and solar inverters. These converters have two unique topologies: voltage source inverters and current source inverters. Voltage source inverters (VSIs) are named for their independently regulated output, which is a voltage waveform. Similarly, current source inverters (CSIs) differ in that the regulated AC output is a current waveform.

Power switching devices, which are typically completely programmable semiconductor power switches, produce DC to AC power conversion. As a result, the output waveforms have abrupt transitions rather than gradual ones as they are composed of discrete numbers. Even a crude approximation of the AC power's sinusoidal waveform works well for some applications. When a nearly sinusoidal waveform is needed, the switching components are run at a rate significantly faster than the intended output frequency, and their duration in each state is regulated to provide an average output that is almost sinusoidal. The carrier-based approach, also known as pulse-width modulation, space-vector technique, and selective-harmonic technique are examples of common modulation techniques.

In single-phase and three-phase applications, voltage source inverters are useful devices. Single-phase virtual switches with isolation (VSIs) are frequently used in multicell arrangements for power supplies, single-phase UPSs, and complex high-power topologies using half-bridge and full-bridge configurations. Applications requiring sinusoidal voltage waveforms, such ASDs, UPSs, and some FACTS devices like the STATCOM, employ three-phase VSIs. Additionally, they are employed in situations where arbitrary voltages are necessary, such as in voltage compensators and active power filters.

A DC current supply can be converted into an AC output current using current source inverters. When using three phases and needing high-quality voltage waveforms, this kind of inverter makes sense.

Multilevel inverters are a relatively new kind of inverters that are gaining a lot of attention. Because power switches on CSIs and VSIs link to either the positive or negative DC bus, they are considered two-level inverters when operating

|e-ISSN: 2319-8753, p-ISSN: 2347-6710| www.ijirset.com | Impact Factor: 8.423| A Monthly Peer Reviewed & Refereed Journal |

|| Volume 13, Issue 5, May 2024 ||

| DOI:10.15680/IJIRSET.2024.1305357 |

normally. The AC output might more closely resemble a sine wave if the inverter output terminals had access to more than two voltage levels. Because of this, multiple inverters provide better performance despite being more expensive and complicated.

The DC links that are utilized and whether or not freewheeling diodes are necessary vary depending on the kind of inverter. Depending on how it will be used, either can be configured to work in pulse-width modulation (PWM) or square-wave mode. While PWM may be implemented in a variety of ways and yields waveforms of greater quality, square-wave mode is simpler.

2.11.3 Voltage source inverter

The output inverter portion is fed by Voltage Source Inverters (VSI) from a source with a voltage that is roughly constant.

The choice of modulation technique for a specific application depends on the desired quality of the current output waveform. A VSI's output is made up of discrete values. The loads must be inductive at the chosen harmonic frequencies to provide a smooth current waveform. When a capacitive load is connected without any kind of inductive filtering between the source and the load, the load will experience a choppy current waveform with big, frequent current spikes.

There are three main types of VSIs:

- Single-phase half-bridge inverter
- Single-phase full-bridge inverter
- Three-phase voltage source inverter

2.11.4 Single-phase half-bridge inverter

Half-bridge inverters with a single-phase voltage source are frequently used in power supplies and are designed for lower voltage applications. This inverter's circuit design is seen in Figure 1.

When the inverter operates, low-order current harmonics are pumped back into the source voltage. This indicates that this design requires two large capacitors for filtering. In each leg of the inverter, only one switch may be activated at a time, as shown in Figure 1. The DC source would be shorted out if both switches in a leg were turned on simultaneously.

Multiple modulation strategies are available to inverters for controlling their switching schemes. The AC output waveform, vc, is compared to a carrier voltage signal, vΔ, using the carrier-based PWM approach. S+ is on when vc exceeds vΔ, while S- is on when vc is less than vΔ. The PWM becomes a specific sinusoidal instance of the carrier-based PWM when the triangle carrier signal is at frequency fΔ with its amplitude at vΔ and the AC output is at frequency fc with its amplitude at vc. [4] We refer to this situation as sinusoidal pulse-width modulation, or SPWM. Ma = vc/vΔ is the definition of the modulation index, often known as the amplitude-modulation ratio, for this.

The formula mf = fΔ/fc is used to get the normalized carrier frequency, often known as the frequency-modulation ratio. At the expense of saturation, a larger fundamental AC output voltage will be seen if the over-modulation area, ma, is greater than one. The output waveform's harmonics for SPWM have well specified amplitudes and frequency. As a result, the filtering components required for the low-order current harmonic injection from the inverter's operation are designed more simply. In this mode of operation, the maximum output amplitude is equal to half of the source voltage. A square wave appears on the inverter's output waveform if the maximum output amplitude, ma, is greater than 3.24.

As was true for PWM, both switches in a leg for square wave modulation cannot be turned on at the same time, as this would cause a short across the voltage source. The switching scheme requires that both S+ and S- be on for a half cycle of the AC output period.[4] The fundamental AC output amplitude is equal to $vo1 = V_aN = 2vi/\pi$.

Its harmonics have an amplitude of $V_{oh} = V_o1/h$. Therefore, the AC output voltage is not controlled by the inverter, but rather by the magnitude of the DC input voltage of the inverter.

Using selective harmonic elimination (SHE) as a modulation technique allows the switching of the inverter to selectively eliminate intrinsic harmonics. The fundamental component of the AC output voltage can also be adjusted within a desirable range. Since the AC output voltage obtained from this modulation technique has odd half and odd quarter wave symmetry, even harmonics do not exist. Any undesirable odd (N-1) intrinsic harmonics from the output waveform can be eliminated.

|e-ISSN: 2319-8753, p-ISSN: 2347-6710| www.ijirset.com | Impact Factor: 8.423| A Monthly Peer Reviewed & Refereed Journal |

|| Volume 13, Issue 5, May 2024 ||

| DOI:10.15680/IJIRSET.2024.1305357 |

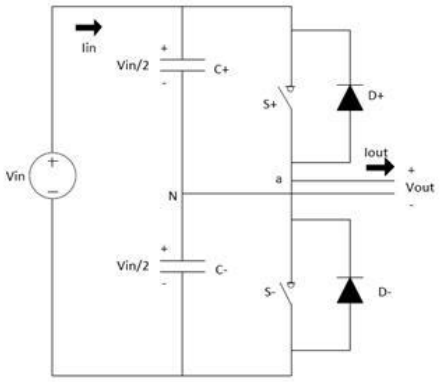

Figure 18. Single-Phase Half-Bridge Voltage Source Inverter

2.12 Single-phase full-bridge inverter

The full-bridge inverter is similar to the half bridge-inverter, but it has an additional leg to connect the neutral point to the load. Figure 2 shows the circuit schematic of the single-phase voltage source full-bridge inverter.

To avoid shorting out the voltage source, S1+ and S1- cannot be on at the same time, and S2+ and S2- also cannot be on at the same time. Any modulating technique used for the full-bridge configuration should have either the top or the bottom switch of each leg on at any given time. Due to the extra leg, the maximum amplitude of the output waveform is Vi, and is twice as large as the maximum achievable output amplitude for the half-bridge configuration.

States 1 and 2 from Table 2 are used to generate the AC output voltage with bipolar SPWM. The AC output voltage can take on only two values, either Vi or –Vi. To generate these same states using a half-bridge configuration, a carrier-based technique can be used. S+ being on for the half-bridge corresponds to S1+ and S2- being on for the full-bridge. Similarly, S- being on for the half-bridge corresponds to S1- and S2+ being on for the full bridge. The output voltage for this modulation technique is more or less sinusoidal, with a fundamental component that has an amplitude in the linear region of less than or equal to one $v_{o1} = v_{ab1} = v_i \bullet ma$.

Unlike the bipolar PWM technique, the unipolar approach uses states 1, 2, 3 and 4 from Table 2 to generate its AC output voltage. Therefore, the AC output voltage can take on the values V_i, 0 or $–V_i$. To generate these states, two sinusoidal modulating signals, V_c and $–V_c$, are needed, as seen in Figure 2.
V_c is used to generate V_aN, while $–V_c$ is used to generate V_bN. The following relationship is called unipolar carrier-based SPWM $v_{o1} = 2 \bullet v_aN_1 = vi \bullet ma$.

The phase voltages V_aN and V_bN are identical, but 180 degrees out of phase with each other. The output voltage is equal to the difference of the two-phase voltages, and do not contain any even harmonics. Therefore, if mf is taken, even the AC output voltage harmonics will appear at normalized odd frequencies, fh. These frequencies are centered on double the value of the normalized carrier frequency. This particular feature allows for smaller filtering components when trying to obtain a higher quality output waveform.

As was the case for the half-bridge SHE, the AC output voltage contains no even harmonics due to its odd half and odd quarter wave symmetry.

|e-ISSN: 2319-8753, p-ISSN: 2347-6710| www.ijirset.com | Impact Factor: 8.423| A Monthly Peer Reviewed & Refereed Journal |

|| Volume 13, Issue 5, May 2024 ||

| DOI:10.15680/IJIRSET.2024.1305357 |

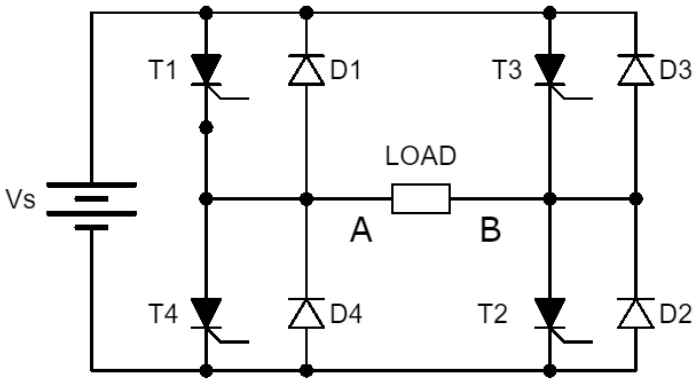

Figure 19. Single-Phase Voltage Source Full-Bridge Inverter

2.13 Three-phase voltage source inverter

Single-phase VSIs are used primarily for low power range applications, while three-phase VSIs cover both medium and high power range applications.[4] Figure 5 shows the circuit schematic for a three-phase VSI.

Switches in any of the three legs of the inverter cannot be switched off simultaneously due to this resulting in the voltages being dependent on the respective line current's polarity. States 7 and 8 produce zero AC line voltages, which result in AC line currents freewheeling through either the upper or the lower components. However, the line voltages for states 1 through 6 produce an AC line voltage consisting of the discrete values of Vi, 0 or –Vi.

For three-phase SPWM, three modulating signals that are 120 degrees out of phase with one another are used in order to produce out of phase load voltages. In order to preserve the PWM features with a single carrier signal, the normalized carrier frequency, mf, needs to be a multiple of three. This keeps the magnitude of the phase voltages identical, but out of phase with each other by 120 degrees. The maximum achievable phase voltage amplitude in the linear region, ma less than or equal to one, is v_{phase} = vi / 2. The maximum achievable line voltage amplitude is Vab1 = v_{ab} • √3 / 2

The only way to control the load voltage is by changing the input DC voltage.

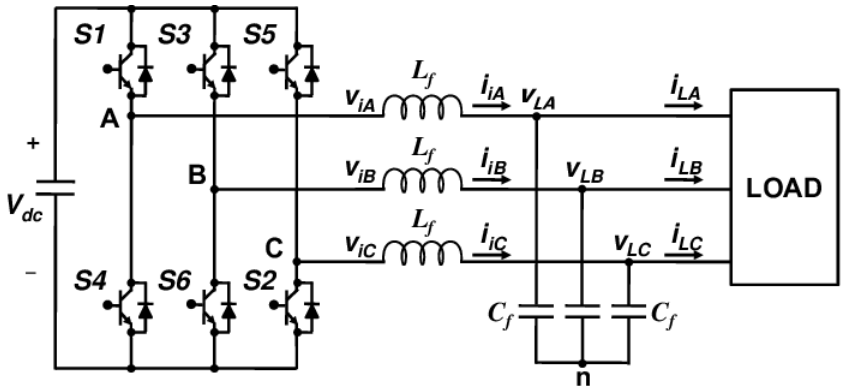

Figure 20. Three-Phase Voltage Source Inverter Circuit Schematic

|e-ISSN: 2319-8753, p-ISSN: 2347-6710| www.ijirset.com | Impact Factor: 8.423| A Monthly Peer Reviewed & Refereed Journal |

|| Volume 13, Issue 5, May 2024 ||

| DOI:10.15680/IJIRSET.2024.1305357 |

III. ADAPTIVE NETWORK BASED FUZZY INFERENCE SYSTEM

3.1 Introduction

The data-driven process known as the adaptive network based fuzzy inference system (ANFIS) represents a neural network method for function approximation problem solving. Typically, data-driven methods for creating ANFIS networks include clustering a training set of numerical samples of the unknown function that has to be approximated. Since its establishment, rule-based process control, pattern recognition, and classification tasks have been effectively handled by ANFIS networks. The fuzzy model presented by Takagi, Sugeno, and Kang in this instance forms the basis of a fuzzy inference system, which is a methodical way to produce fuzzy rules from an input-output data set.

3.2 ANFIS structure

The fuzzy inference system under study is considered to have two inputs and one output for the sake of simplicity. The fuzzy if-then rules of Takagi and Sugeno's kind are contained in the rule base in the following manner:

If x is A and y is B, then z is f(x,y), where z = f(x, y) is a crisp function in the consequent and A and B are the fuzzy sets in the antecedents. The polynomial f(x, y) for the input variables x and y is typically what it is. However, it might also be any other function that can roughly characterize the system's output inside the fuzzy region that the antecedent specifies. A zero order Sugeno fuzzy model, which may be thought of as a particular instance of the Mamdani fuzzy inference system [144], where each rule consequent is described by a fuzzy singleton, is generated when f(x,y) is a constant. A Sugeno fuzzy model of first order is generated if f(x,y) is assumed to be a first order polynomial. In a Sugeno fuzzy inference system of first order with two rules, the two rules might be,

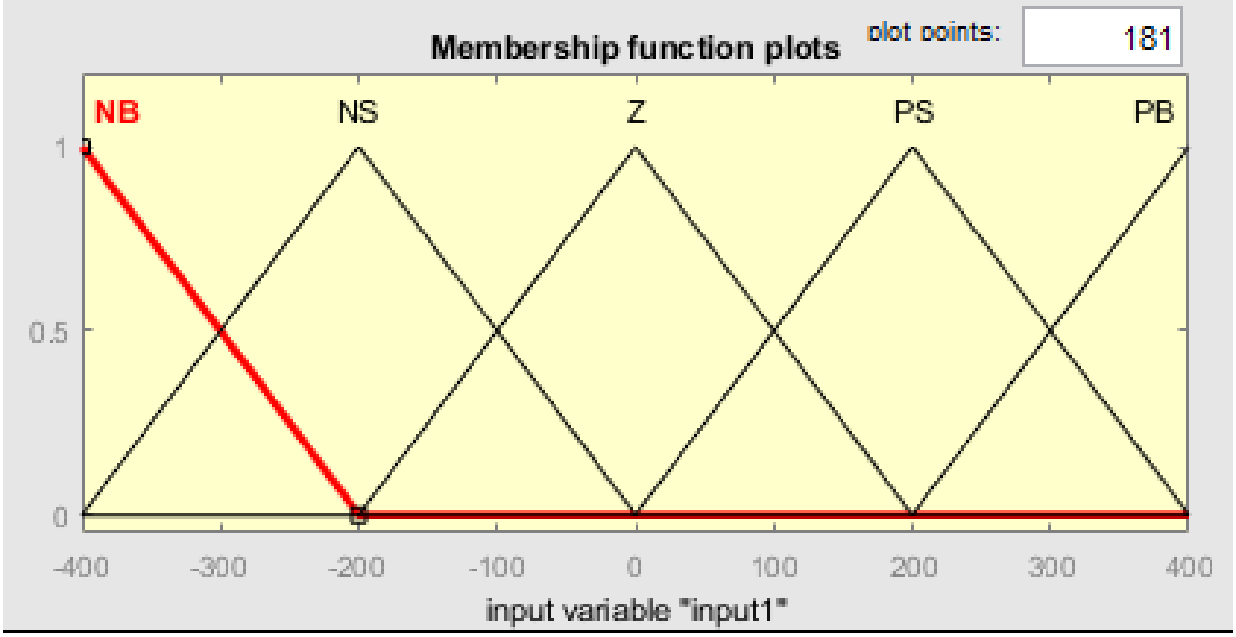

INPUT-1

|e-ISSN: 2319-8753, p-ISSN: 2347-6710| www.ijirset.com | Impact Factor: 8.423| A Monthly Peer Reviewed & Refereed Journal |

|| Volume 13, Issue 5, May 2024 ||

| DOI:10.15680/IJIRSET.2024.1305357 |

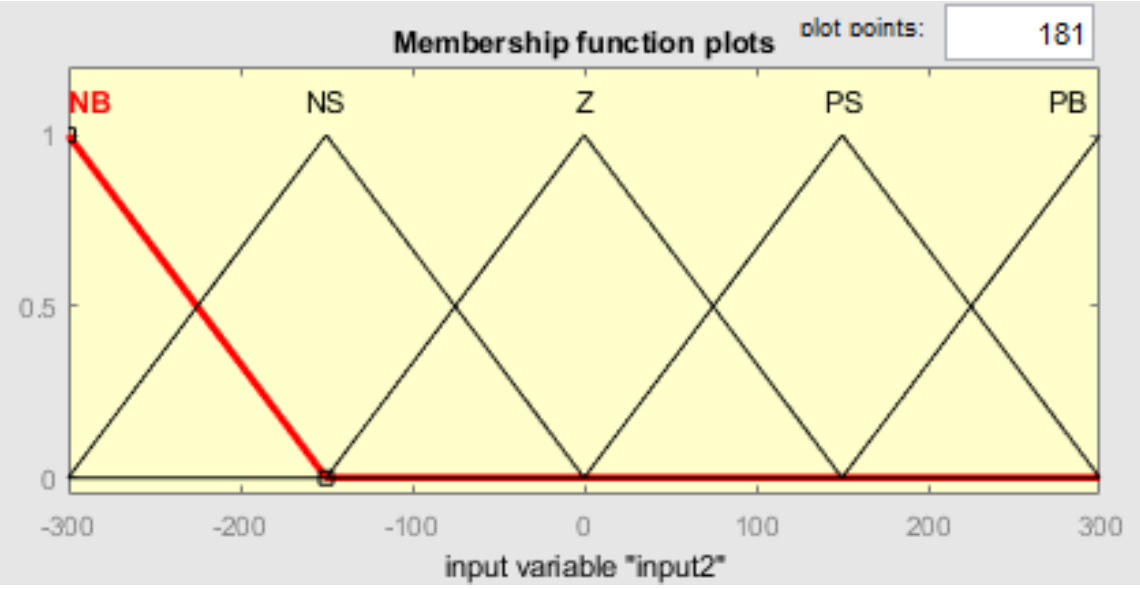

INPUT-2

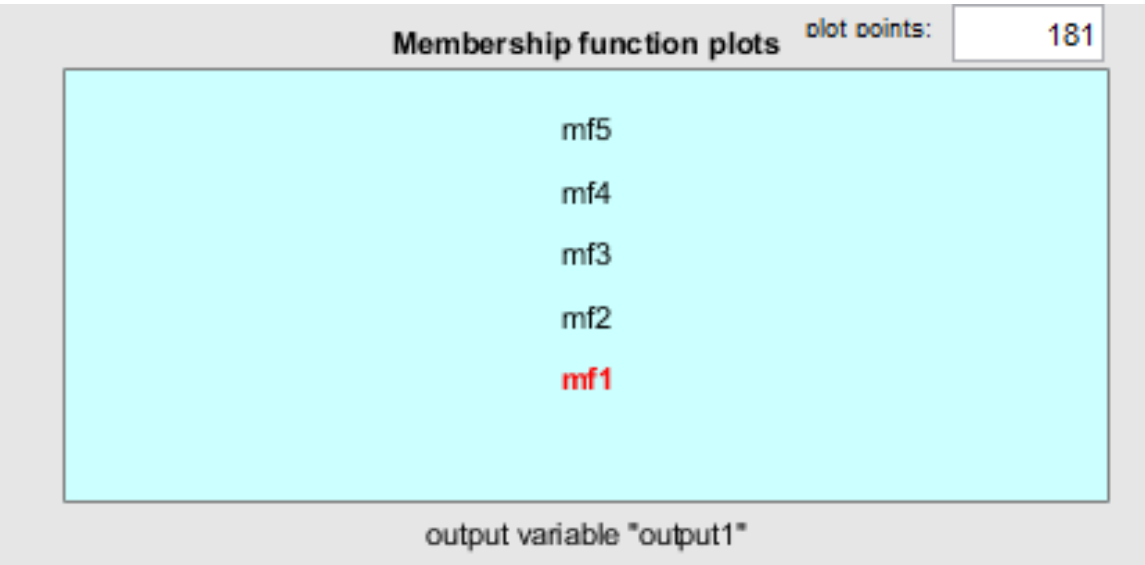

OUTPUT stated as:

Table IF INPUT-1 & 2	OUTPUT
NB	MF1
NS	MF2
Z	MF3
PS	MF4
PB	MF5

Table 6. Output of ANFIS Membership

RULES

- Rule 1: If x is A1 and y is B1 then $f_1 = p_1x + q_1y + r_1$
- Rule 2: If x is A2 and y is B2 then $f_2 = p_2x + q_2y + r_2$

|e-ISSN: 2319-8753, p-ISSN: 2347-6710| www.ijirset.com | Impact Factor: 8.423| A Monthly Peer Reviewed & Refereed Journal |

|| Volume 13, Issue 5, May 2024 ||

| DOI:10.15680/IJIRSET.2024.1305357 |

Here, Takagi and Sugeno's type-3 fuzzy inference method is applied. Each rule's output in this inference system is a linear combination of the input variables plus a constant term. The weighted average of the results from each rule is the final output. Fig. 4.5 displays the comparable equivalent ANFIS structure.

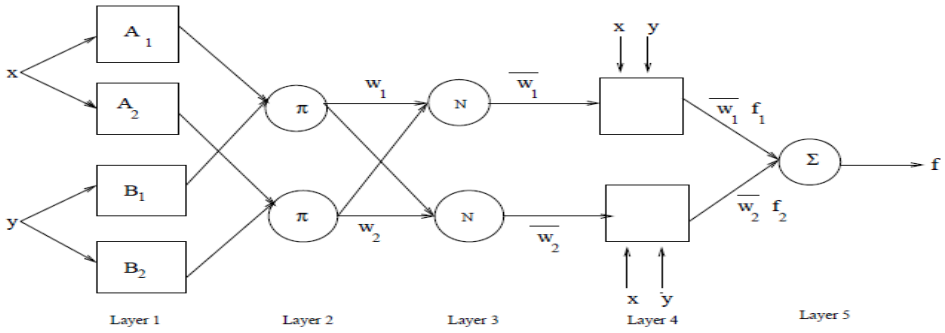

Figure 21. Type-3 ANFIS Structure

The individual layers of this ANFIS structure are described below:
Layer 1: Every node i in this layer is adaptive with a node function

$$O_i^1 = \mu A_i(x)$$

where, x is the input to node i, Ai is the linguistic variable associated with this node function and μA_i is the membership function of Ai. Usually $\mu A_i(x)$ is chosen as

$$\mu A_i(x) = \frac{1}{1 + \left[\left(\frac{x - c_i}{a_i}\right)^2\right]^{b_i}}$$

Or,

$$\mu A_i(x) = exp\left\{-\left(\frac{x - c_i}{a_i}\right)^2\right\}$$

where, x is the input and {ai, bi, ci} is the premise parameter set.
Layer 2: Every fixed node in this layer determines the firing strength using a rule. Every node's output is determined by multiplying all of the signals that arrive at it,

$$O_i^2 = w_i = \mu A_i(x) \times \mu B_i(y), \quad i = 1,2$$

Layer 3: In this layer, each node is fixed. The ratio of the firing strength of the ith rule to the total firing strength of all the rules is computed by each ith node. The normalized firing strength provided by is the output of the ith node.

$$O_i^3 = \overline{w_i} = \frac{w_i}{w_1 + w_2}, \quad i = 1,2$$

Layer 4: With a node function provided by, each node in this layer is adaptable.

$$O_i^4 = \overline{w_i} f_i = \overline{w_i}\,(p_i x + q_i y + r_i), \quad i = 1,2$$

Where, w_i is the output of Layer 3 and {pi, qi, ri} is the consequent parameter set.
Layer 5: This layer comprises of only one fixed node that calculates the overall output as the summation of all incoming signals, i.e.

$$O_i^5 = overall\ output = \sum_i \overline{w_i} f_i = \frac{\sum_i w_i f_i}{\sum_i w_i}$$

3.3 Learning Algorithm
In the ANFIS structure, it is observed that given the values of premise parameters, the final output can

|e-ISSN: 2319-8753, p-ISSN: 2347-6710| www.ijirset.com | Impact Factor: 8.423| A Monthly Peer Reviewed & Refereed Journal |

|| Volume 13, Issue 5, May 2024 ||

| DOI:10.15680/IJIRSET.2024.1305357 |

be expressed as a linear combination of the consequent parameters. The output f in Fig. 4.1 can be written as

$$f = \frac{w_1}{w_1 + w_2} f_1 + \frac{w_2}{w_1 + w_2} f_2$$
$$= \overline{w_1} f_1 + \overline{w_2} f_2$$
$$= (\overline{w_1} x) p_1 + (\overline{w_1} y) q_1 + (\overline{w_1}) r_1 + (\overline{w_2} x) p_2 + (\overline{w_2} y) q_2 + (\overline{w_2}) r_2$$

where f is linear in the consequent parameters (p1, q1, r1, p2, q2, r2).
The least squares estimate is used in the learning algorithm's forward pass to identify subsequent parameters. The error signals travel backward from the output layer to the input layer during the backward pass. These error signals are the derivatives of the squared error with respect to each node output. The gradient descent technique updates the premise parameters on this backward run.

3.4 Derivation of the Initial Fuzzy Model
As previously said, finding the best fuzzy model in relation to the training data in ANFIS-based system modeling given a collection of rules with defined premise parameters simplifies to a linear least-squares estimate issue. S.L. Chiu [77] presented a quick and reliable technique for identifying fuzzy models from input-output data. This approach uses a least squares estimation technique in conjunction with the cluster estimation method to identify the critical input variables while creating a fuzzy model from data. There are two phases in the method: i) The first stage is to use a cluster estimation approach that incorporates all available input variables to generate an initial fuzzy model from the input output data. ii) The following stage involves determining which input variables are crucial by evaluating each variable's importance in the first fuzzy model.

3.5 Extracting the initial fuzzy model
The first step in the modeling procedure is to derive a fuzzy model. The purpose of this model is to determine how many inputs, linguistic variables, and ultimately rules there will be in the finished fuzzy model. Before the final optimum model can be constructed, the initial model must also choose the model selection criteria and the input variables for the final model. Based on the fuzzy rules, the subtractive clustering methodology [145] or the grid partitioning method can be used to choose this initial fuzzy model. [74] [68, 91].

3.5.1 Subtractive Clustering Technique
This approach is applied to the input output data pairs collected from the system that has to be modeled in order to derive the first fuzzy model via subtractive clustering. Finding the cluster centers of the input-output data pairs is made easier with the use of the cluster estimation approach. Because each cluster center indicates the presence of a rule, this in turn aids in the determination of the rules that are dispersed throughout the input-output space. Furthermore, it aids in ascertaining the values of the premise parameters. This is significant because, during a neural network training session, a model that starts out extremely near to the end value will eventually quickly converge towards that value. The potentials of each input and output data point in this clustering approach are determined as functions of their Euclidian distances from each other. Cluster centers are defined as sites with a potential greater than a certain threshold. The first fuzzy model may be recovered when the cluster centers are determined because they will also indicate the number of linguistic variables. Below is a quick description of the cluster estimate approach for figuring out the number of rules and initial rule parameters [77]. Examining an M-dimensional space, we have n data points {x1, x2, ..., xn}. It is expected that each dimension's data points have been normalized to the point where a unit hypercube surrounds them. Every single data point is regarded as a possible cluster center. Pi is defined as a measurement of data point xi's propensity to act as a cluster center.

$$P_i = \sum_{j=1}^{n} e^{-\alpha ||x_i - x_j||^2}$$

Where, $\alpha = \frac{4}{r_a^2}$ and ||. || denotes the Euclidean distance and r_a is a positive constant. As a result, a data point's potential is determined by how far away it is from every other data point. The radius that defines a neighborhood in this case is ra. The potential is not much affected by data points outside of this range. The data point with the highest potential is chosen as the first cluster center once each data point's potential has been calculated. Let P_1 be the potential value of the first cluster center, and let x_1 be its position. Next, the formula modifies each data point xi's potential.

|e-ISSN: 2319-8753, p-ISSN: 2347-6710| www.ijirset.com | Impact Factor: 8.423| A Monthly Peer Reviewed & Refereed Journal |

|| Volume 13, Issue 5, May 2024 ||

| DOI:10.15680/IJIRSET.2024.1305357 |

$$P_i = P_i - P_1^* e^{-ß||x_i - x_1^*||^2}$$

$$ß = \frac{4}{r_b^2}$$

and the constant rb is positive. As a result, each data point has potential deducted from it based on how far away it is from the cluster center. The neighborhood's quantifiable potential reduction is defined by the constant rb, which is essentially its radius. The often-selected value is rb = 1.25ra [77]. The data point with the largest residual potential is chosen as the second cluster center once all data points' potentials have been adjusted in accordance with Eq. 4.3.3. Each data point's potential is further diminished based on how far away it is from the second cluster center. Generally speaking, the formula modifies each data point's potential once the kth cluster center has been determined.

$$P_i = P_i - P_k^* e^{-ß||x_i - x_k^*||^2}$$

where x_k is the location of the kth cluster center and P_k is the potential value.
The process of acquiring new cluster center and revising potentials repeats until the stopping criterion $P_k < 0.15P_1$ is satisfied. Each cluster center as derived Essentially, the data point above characterizes an input-output behavior characteristic of the system we want to simulate. As a result, a rule that characterizes the behavior of the system may be built around each cluster center.

In an M-dimensional space, $\{x_1, x_2, ..., x_c\}$ is seen as a collection of c cluster centers. Once more, it is believed that input variables correlate to the first N dimensions and output variables to the last M − N dimensions. Every vector x_i may be divided into two component vectors, y_i and z, where y_i represents the cluster center's location in input space and z_i represents its location in output space. Consequently, x_i might be represented as

$$x_i^* = [y_i^*; z_i^*]$$

All cluster centers, xi, are regarded as fuzzy rules. To characterize the behavior of the system, if input is around yi, then output is near zi. The degree to which rule I is satisfied given an input vector y is specified as

$$\mu_i = e^{-\alpha ||y - y_i^*||^2}$$

where _ is a constant defined by Eq. 4.3.2. Output vector z is computed as

$$z = \frac{\sum_{i=1}^{c} \mu_i z_i^*}{\sum_{i=1}^{c} \mu_i}$$

This computational scheme can be thought of as an fuzzy if-then rule-based inference system. The format of each rule is as follows:
Where Yj is the jth input variable and Zj is the jth output variable; Aij is an exponential membership function in the ith rule with the jth input and Bij is a singleton in the ith rule associated with the jth output. IF Y1 is Ai1 and Y2 is Ai2 and... THEN Z1 is Bi1 and Z2 is Bi2... Aij and Bij are provided for the ith rule, which is represented by cluster center xi by:

$$A_{ij}(Y_j) = e^{-0.5(\frac{Y_j - y_{ij}^*}{\sigma_{ij}})^2}$$

Aij

$$B_{ij} = z_{ij}^*$$

where y_{ij} is the j_{th} element of y_i and z_{ij} is the j^{th} element of z_i; 2_{ij} = 1,2,…

3.5.2 Grid Partitioning Technique

Grid partitioning is a second technique that can be applied to formulate the initial fuzzy model's rules [74] [68, 91]. When there are fewer inputs and their membership functions, this method is employed. To create the antecedents of the fuzzy rules, the input space is divided into several fuzzy regions. Fig. 4.2 displays the Grid partitioned fuzzy space for a two-input model with three membership functions per input. The input space's ordinate and abscissa are

|e-ISSN: 2319-8753, p-ISSN: 2347-6710| www.ijirset.com | Impact Factor: 8.423| A Monthly Peer Reviewed & Refereed Journal |

|| Volume 13, Issue 5, May 2024 ||

| DOI:10.15680/IJIRSET.2024.1305357 |

represented by the two dimensions. The ANFIS methodology created by Jang is then used to optimize the rules derived from either of the two approaches. Using the gradient descent algorithm, the premise membership functions are optimized, and the resulting equations are then optimized using linear least squares estimation.

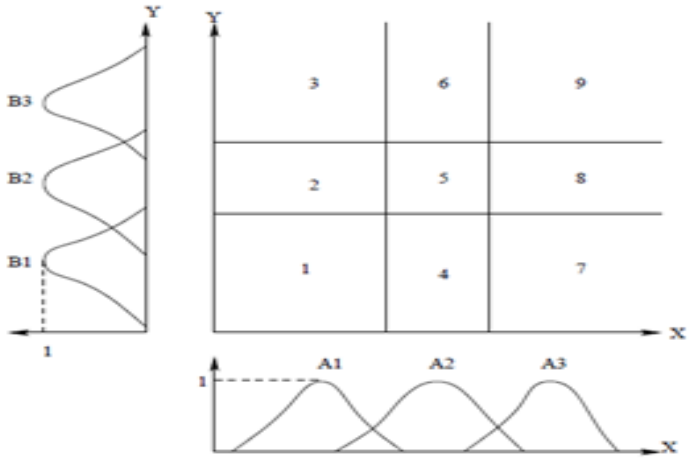

Figure 22. grid partitioned subspaces for a type-3,2-input ANFIS

3.6 Selection of input variables and final fuzzy model

Until the results from every possible combination of the input variables in the model are compared, no matter how good the criteria used for model selection based on some inputs, there is no way to know that the model will produce the best result. However, even with a moderate number of input variables (N), there are still 2N possible combinations of the variables, making this a laborious task. From a modeling perspective, a practical model that is more straightforward, dependable, and application-relevant is produced by including only the significant variables. This is because there will be less variables to measure going forward. The initial fuzzy model can be used to determine the significance of each input variable in order to accomplish this. This has been achieved in the proposed ANFIS model by selecting the model from the models obtained using the following two methods that exhibits the least modeling error.

3.6.1 RMSE Method

Without the need to create new models, the fuzzy rule framework in this method offers a simple way to evaluate the significance of each input variable. The general idea is to take out of the rules all antecedent clauses related to a specific input variable, and then use the checking error criterion to assess the model's performance [77]. By removing another input variable, the process is repeated if this lowers the modeling error. The eliminated variable is kept, and another variable is eliminated in its place, if the modeling error rises. This process is repeated until there is no more extra input variable that can be eliminated to reduce the modeling error. The Root mean square error (RMSE) is the criterion that is used to choose the final fuzzy model. The final model for which the RMSE is the lowest is thought to be the ANFIS structure of the system that is being modeled. Assume, for instance, that the original model contains four inputs and the following rules:

If, Y_1 is A_{i1}, Y_2 is A_{i2}, Y_3 is A_{i3}, Y_4 is A_{i4} then Z_1 is B_{i1}

By temporarily eliminating the antecedent clauses involving Y3, the rules are truncated to the form below, allowing one to test the significance of the Y3 variable in the model:

|e-ISSN: 2319-8753, p-ISSN: 2347-6710| www.ijirset.com | Impact Factor: 8.423| A Monthly Peer Reviewed & Refereed Journal |

|| Volume 13, Issue 5, May 2024 ||

| DOI:10.15680/IJIRSET.2024.1305357 |

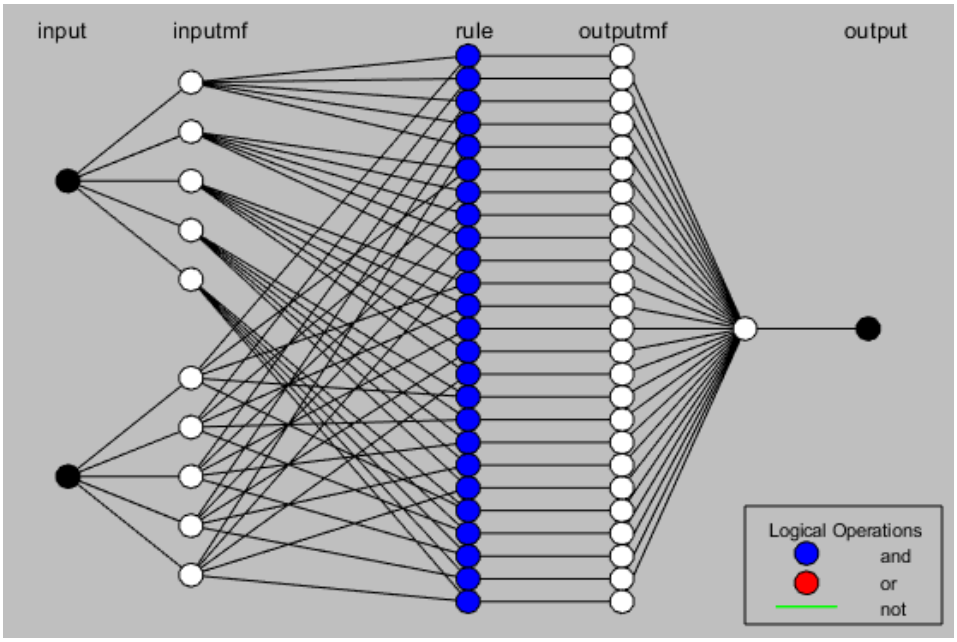

Figure 23. RMSE Neural Network Schematic

3.7 ANFIS Structure

IF Y_1 is A_{i1} and Y_2 is A_{i2} and Y_4 is A_{i4} THEN Z_1 is B_{i1}. Y3 can be excluded from the list of potentially significant variables if the resulting model performance does not deteriorate in relation to the performance measure, which is the RMSE of the output corresponding to an independent set of checking data. Fig. 24 illustrates the variable selection procedure for an initial model with four inputs.

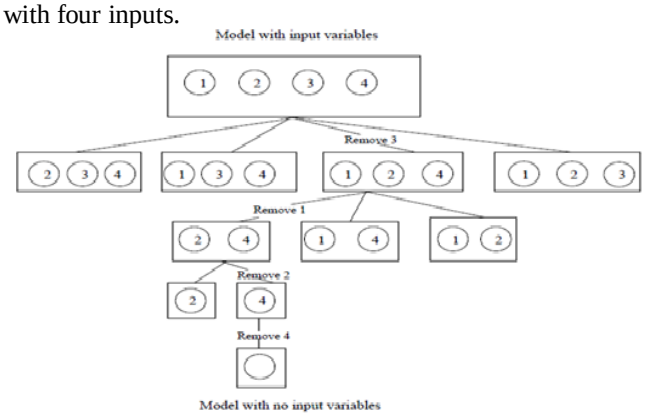

Figure 24. variable selection process for a four-input initial model

3.7.1 Random Combination Method

In order to keep things simple, the second model assumes that ANFIS has just two inputs. Six of the system's historical inputs and four of the system's historical outputs to be modeled make up the set of ten dynamic modeling inputs that are chosen for this purpose. There are 10 potential candidates for dynamic modeling, and for every 6 inputs, there are 4 possible combinations that can result in 4 different outputs. Thus, the number of possible combinations of input candidate pairs will be 6×4 = 24. The following 24 initial fuzzy models will be generated by each of these various combinations:

{x(t-1), y(t-1)}, {x(t-1), y(t-2)}, {x(t-1), y(t-3)}, {x(t-1), y(t-4)}
{x(t-2), y(t-1)}, {x(t-2), y(t-2)}, {x(t-2), y(t-3)}, {x(t-2), y(t-4)}
{x(t-3), y(t-1)}, {x(t-3), y(t-2)}, {x(t-3), y(t-3)}, {x(t-3), y(t-4)}
{x(t-4), y(t-1)}, {x(t-4), y(t-2)}, {x(t-4), y(t-3)}, {x(t-4), y(t-4)}
{x(t-5), y(t-1)}, {x(t-5), y(t-2)}, {x(t-5), y(t-3)}, {x(t-5), y(t-4)}
{x(t-6), y(t-1)}, {x(t-6), y(t-2)}, {x(t-6), y(t-3)}, {x(t-6), y(t-4)}

|e-ISSN: 2319-8753, p-ISSN: 2347-6710| www.ijirset.com | Impact Factor: 8.423| A Monthly Peer Reviewed & Refereed Journal |

|| Volume 13, Issue 5, May 2024 ||

| DOI:10.15680/IJIRSET.2024.1305357 |

The initial fuzzy model is selected from the 24 models mentioned above based on the model with the lowest RMSE. This method allows you to apply either the grid partition-based technique or subtractive clustering to determine the number of membership functions per input. The final model for which the RMSE is the lowest is thought to be the ANFIS structure of the system that is being modeled. The Least Squares Estimation (LSE) algorithm is used to update the subsequent parameters of the initial fuzzy model. Similar to this, a neural network that employs the gradient descent algorithm and the back propagation learning method updates the rules that are derived from clustering or the grid partition-based approach. The optimization of the fuzzy membership's premise parameters results from this updating.

IV. SIMULATION RESULTS

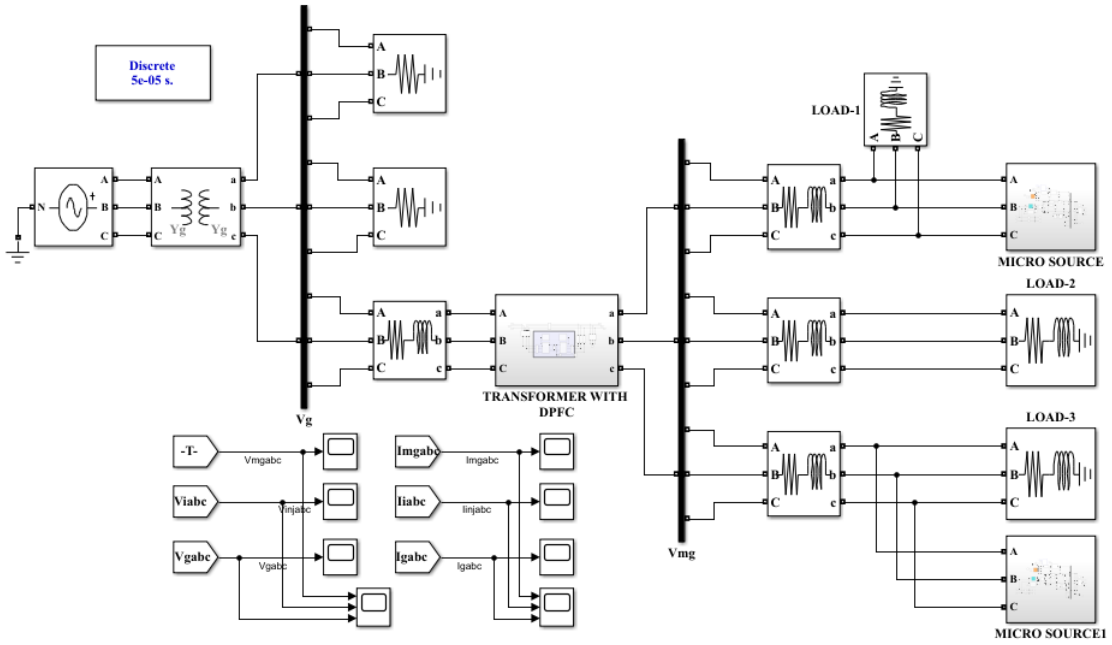

Figure 25. Schematic diagram of Discrete Micro Sources

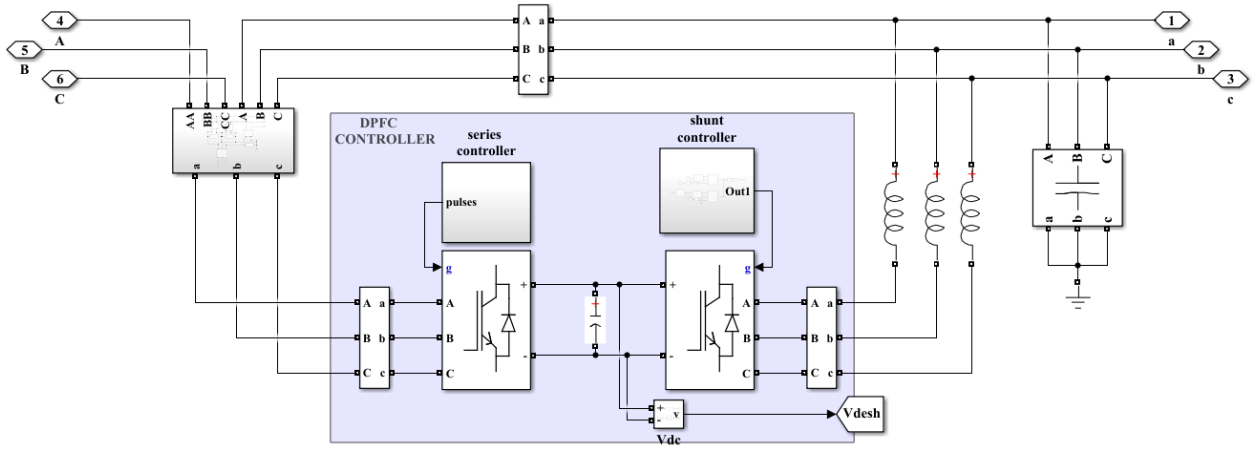

Figure 26. Schematic of DPFC Controller

|e-ISSN: 2319-8753, p-ISSN: 2347-6710| www.ijirset.com | Impact Factor: 8.423| A Monthly Peer Reviewed & Refereed Journal |

|| Volume 13, Issue 5, May 2024 ||

| DOI:10.15680/IJIRSET.2024.1305357 |

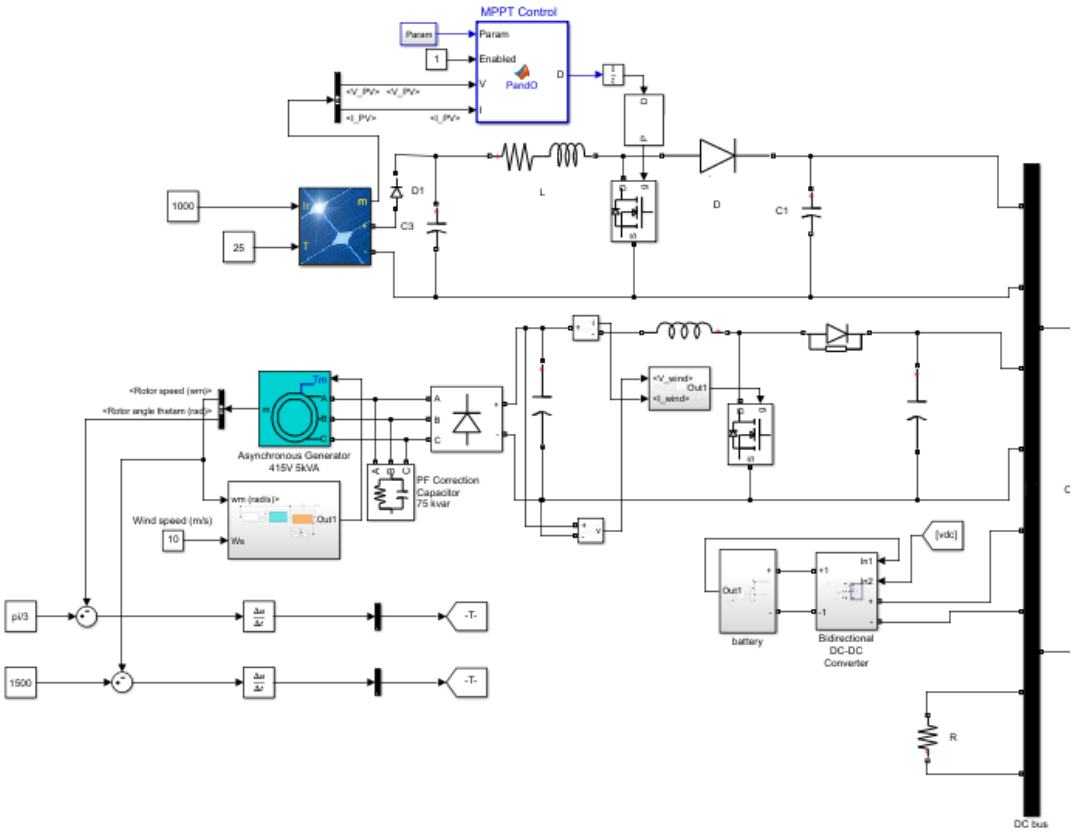

Figure 27. Schematic of Microgrid Source

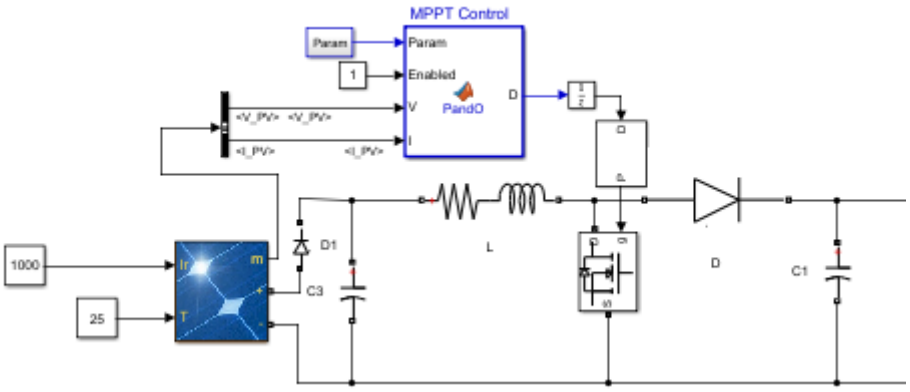

Figure 28. Schematic of Solar power generation

|e-ISSN: 2319-8753, p-ISSN: 2347-6710| www.ijirset.com | Impact Factor: 8.423| A Monthly Peer Reviewed & Refereed Journal |

|| Volume 13, Issue 5, May 2024 ||

| DOI:10.15680/IJIRSET.2024.1305357 |

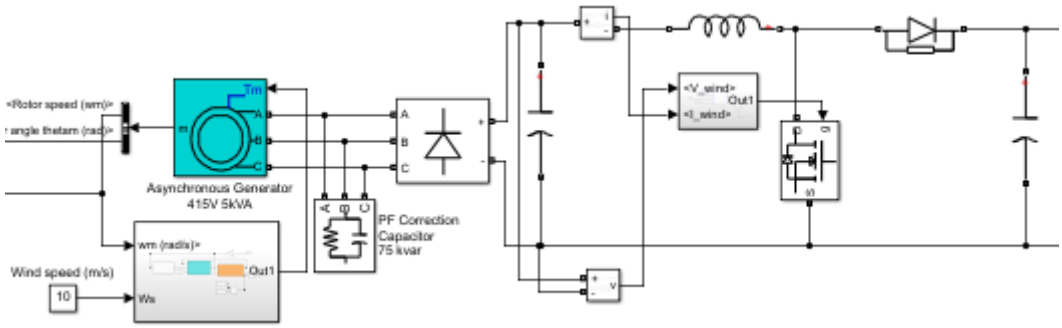

Figure 29. Schematic of Wind power generation

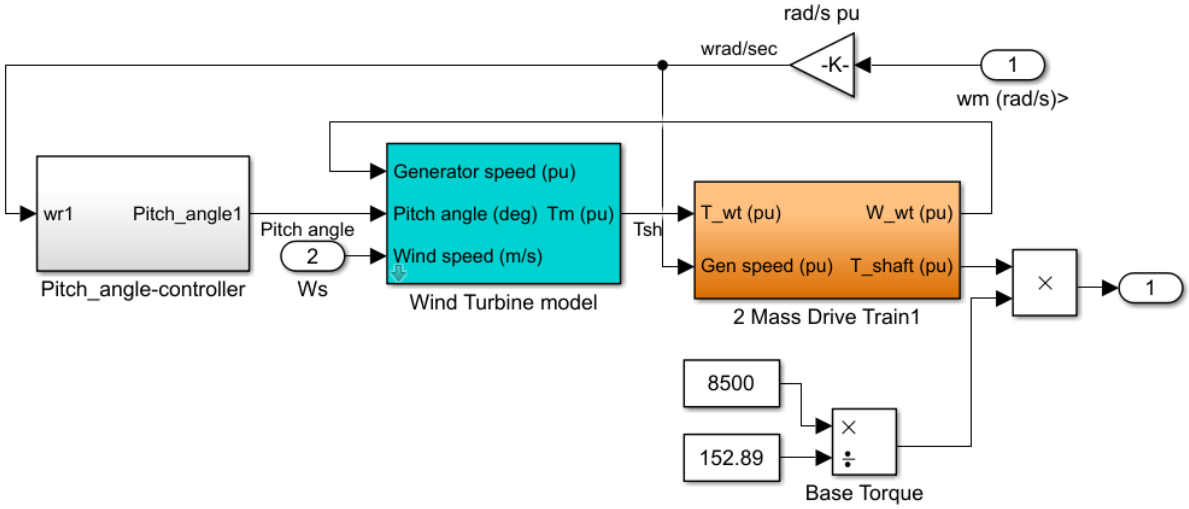

Figure 30. Schematic of Wind Turbine Controller

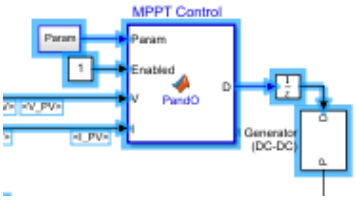

Figure 31. Schematic of Solar Side MPPT Controller

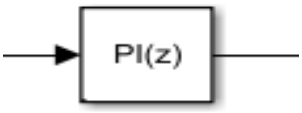

Figure 32. Denomination of PI Controller

International Journal of Innovative Research in Science, Engineering and Technology (IJIRSET)

|e-ISSN: 2319-8753, p-ISSN: 2347-6710| www.ijirset.com | Impact Factor: 8.423| A Monthly Peer Reviewed & Refereed Journal |

|| Volume 13, Issue 5, May 2024 ||

| DOI:10.15680/IJIRSET.2024.1305357 |

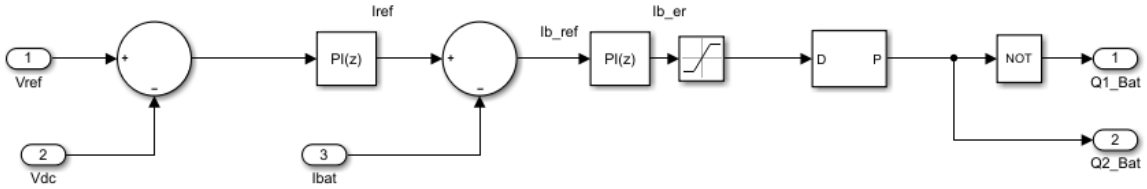

Figure 33. Control map of Bidirectional Converter Controller

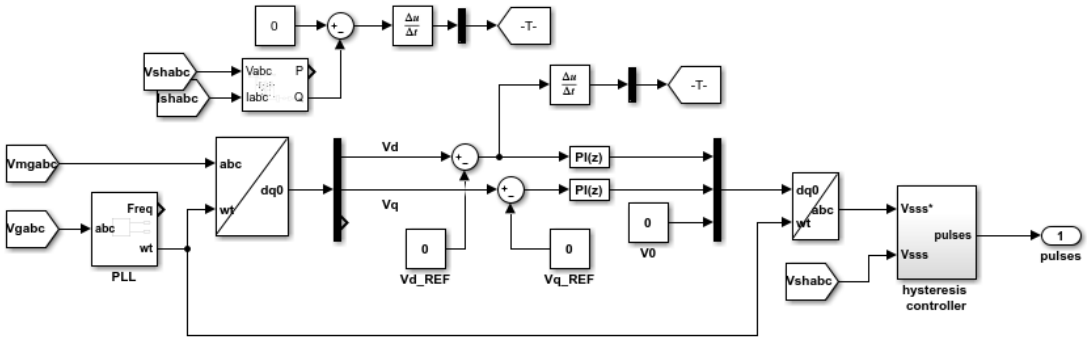

Figure 34. Control Schematic of Series Controller

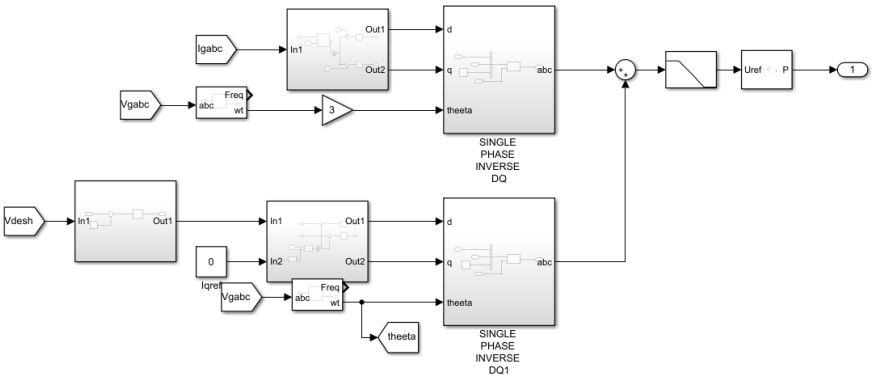

Figure 35. Control Schematic of Shunt Controller

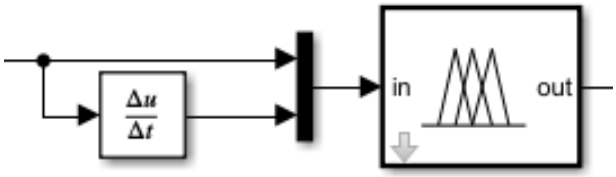

Figure 36. Fuzzy Logic Controller

|e-ISSN: 2319-8753, p-ISSN: 2347-6710| www.ijirset.com | Impact Factor: 8.423| A Monthly Peer Reviewed & Refereed Journal |

|| Volume 13, Issue 5, May 2024 ||

| DOI:10.15680/IJIRSET.2024.1305357 |

4.1 Case 1: Improvement of power quality in a hybrid system using PI Controller

4.1.1 Output waveforms for distorted micro grid voltage, injected voltage, and compensated grid voltage using PIC

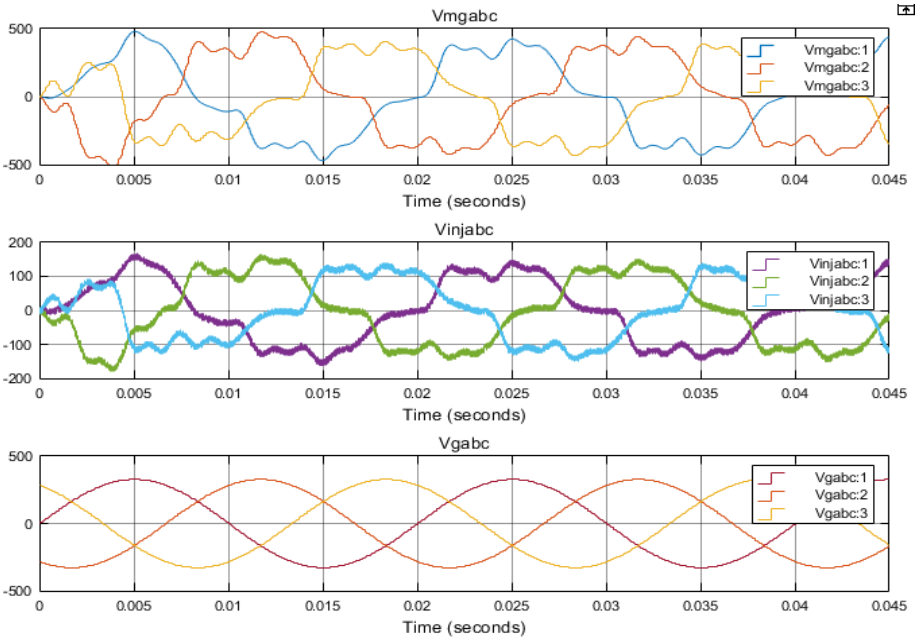

Figure 37. Case 1: Voltage Results using PIC; Vmgabc, Vinjabc, Vgabc

4.1.2 Output waveforms for distorted micro grid current, injected current, and compensated grid current using PI Controller

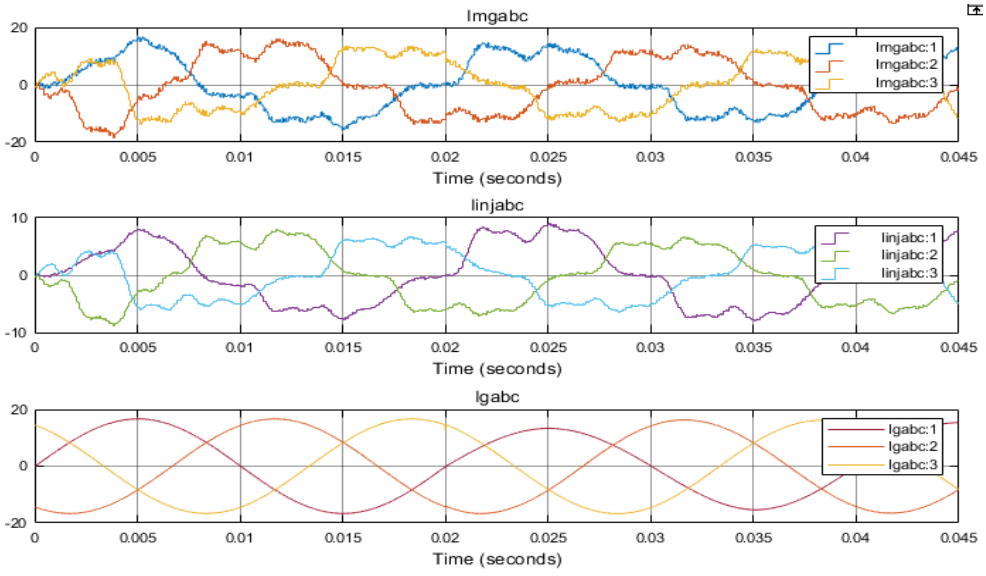

Figure 38. Case 1: Current Results using PIC; Imgcabc, linjabc, lgabc

International Journal of Innovative Research in Science, Engineering and Technology (IJIRSET)

|e-ISSN: 2319-8753, p-ISSN: 2347-6710| www.ijirset.com | Impact Factor: 8.423| A Monthly Peer Reviewed & Refereed Journal |

|| Volume 13, Issue 5, May 2024 ||

| DOI:10.15680/IJIRSET.2024.1305357 |

4.1.3 Output Frequency Results using PI Controller

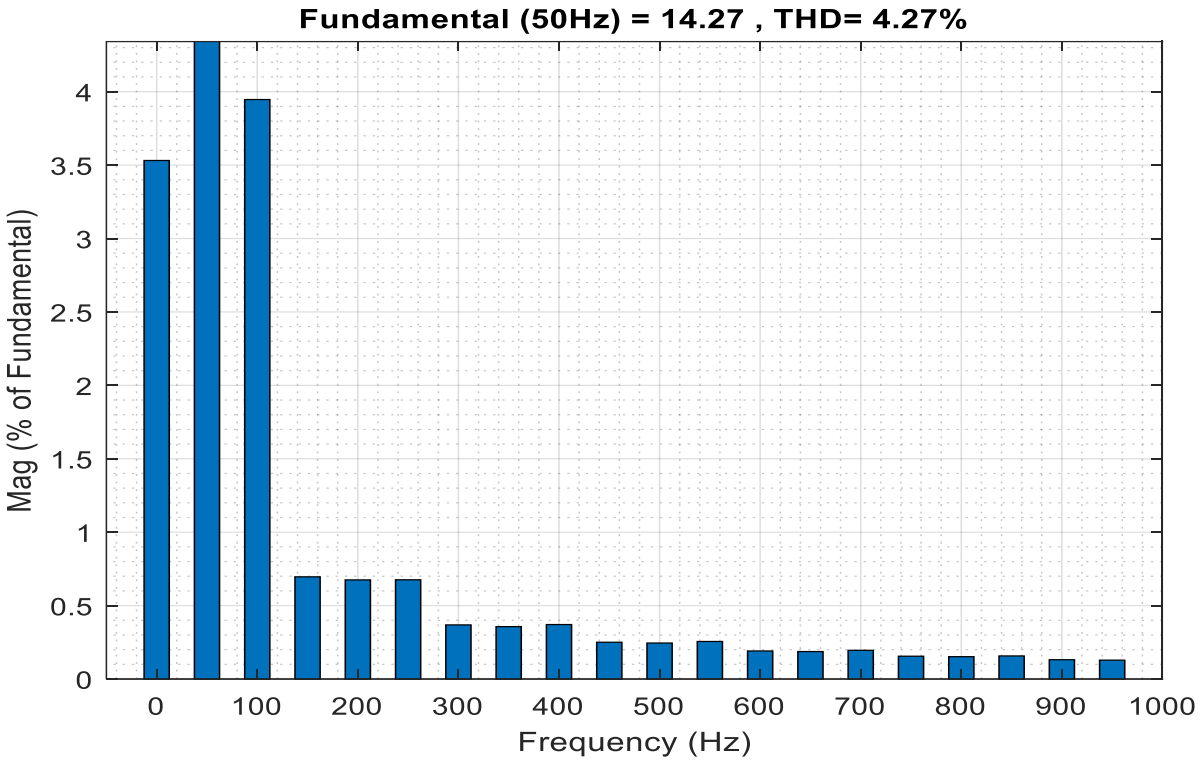

Figure 39. Case 1: Frequency Results; Output using PI Controller

4.2 Case 2: Improvement of power quality in a hybrid system using FLC

4.2.1 Output waveforms for uncompensated micro grid voltage, injected voltage and compensated grid voltage using FLC

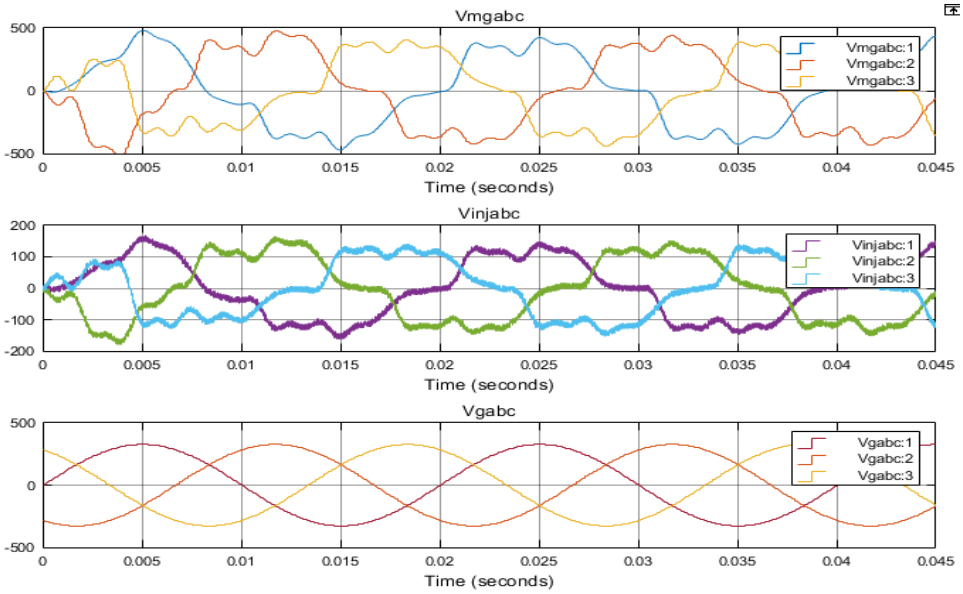

Figure 40. Case 2: Voltage Results using FLC; Vmgabc, Vinjabc, Vgabc

|e-ISSN: 2319-8753, p-ISSN: 2347-6710| www.ijirset.com | Impact Factor: 8.423| A Monthly Peer Reviewed & Refereed Journal |

|| Volume 13, Issue 5, May 2024 ||

| DOI:10.15680/IJIRSET.2024.1305357 |

4.2.2 Output waveforms for uncompensated micro grid current, injected current, and compensated grid current using FLC

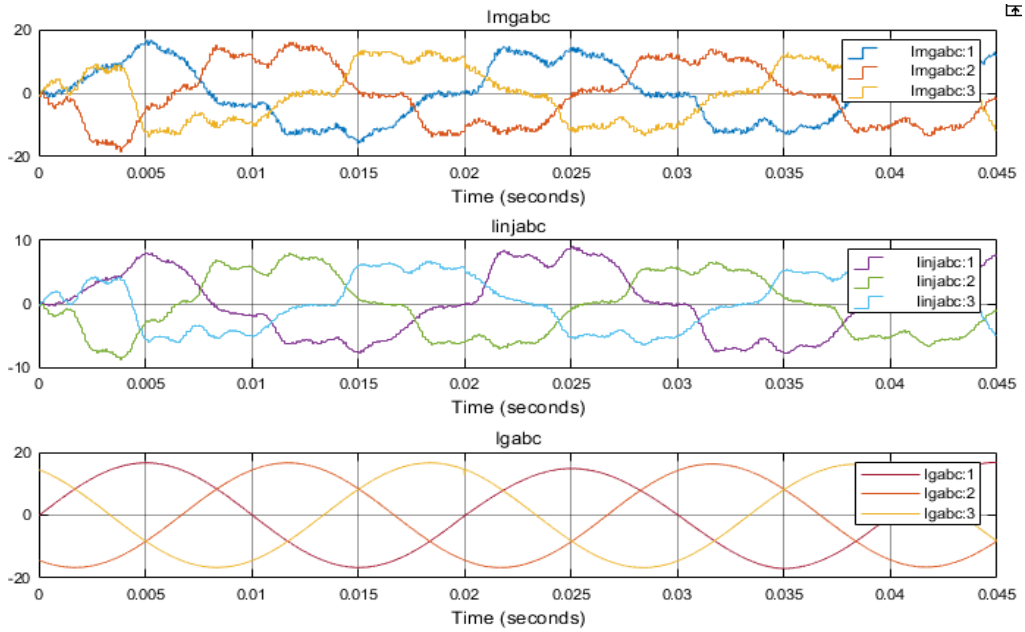

Figure 41. Case 2: Current Results using FLC; Imgcabc, linjabc, lgabc

4.2.3 Output Frequency Results using Fuzzy Logic Controller

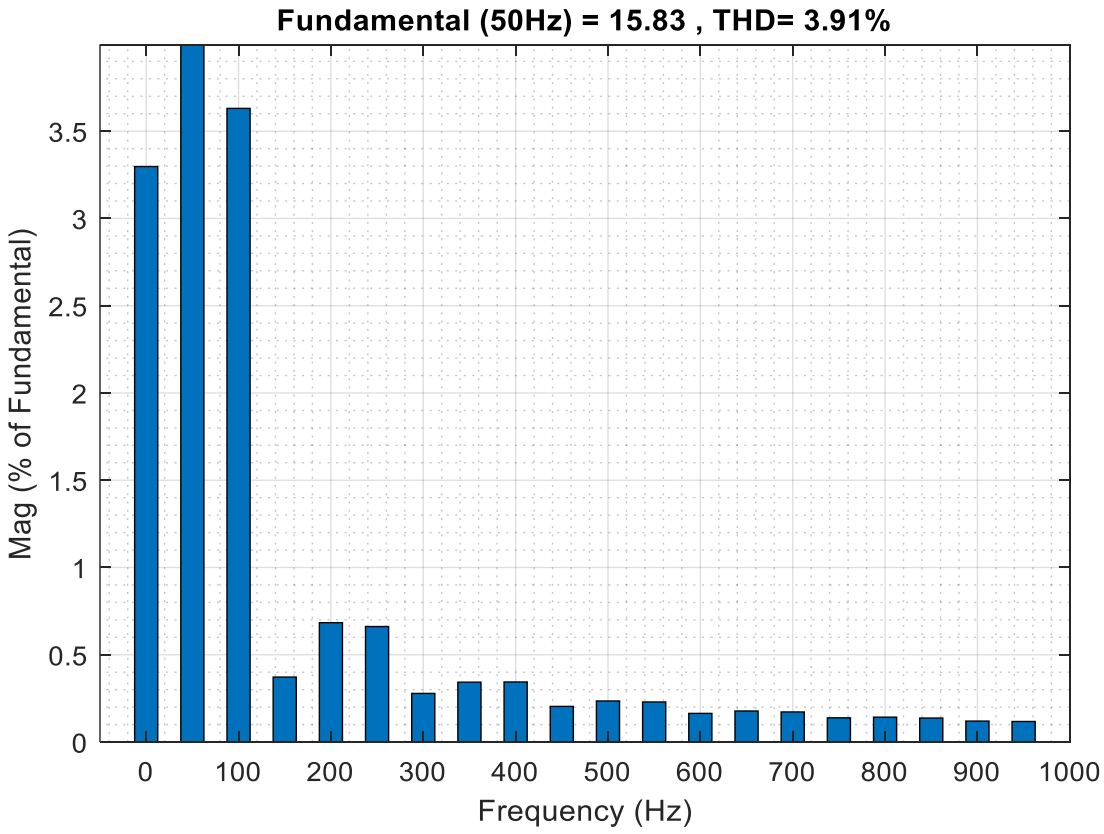

Figure 42. Case 2: Frequency Results; Output using Fuzzy Logic Controller

|e-ISSN: 2319-8753, p-ISSN: 2347-6710| www.ijirset.com | Impact Factor: 8.423| A Monthly Peer Reviewed & Refereed Journal |

|| Volume 13, Issue 5, May 2024 ||

| DOI:10.15680/IJIRSET.2024.1305357 |

4.3 Case 3: Improvement of Transient stability in a hybrid system using PI and FLC DPFC Controllers

4.3.1 Using PI controller

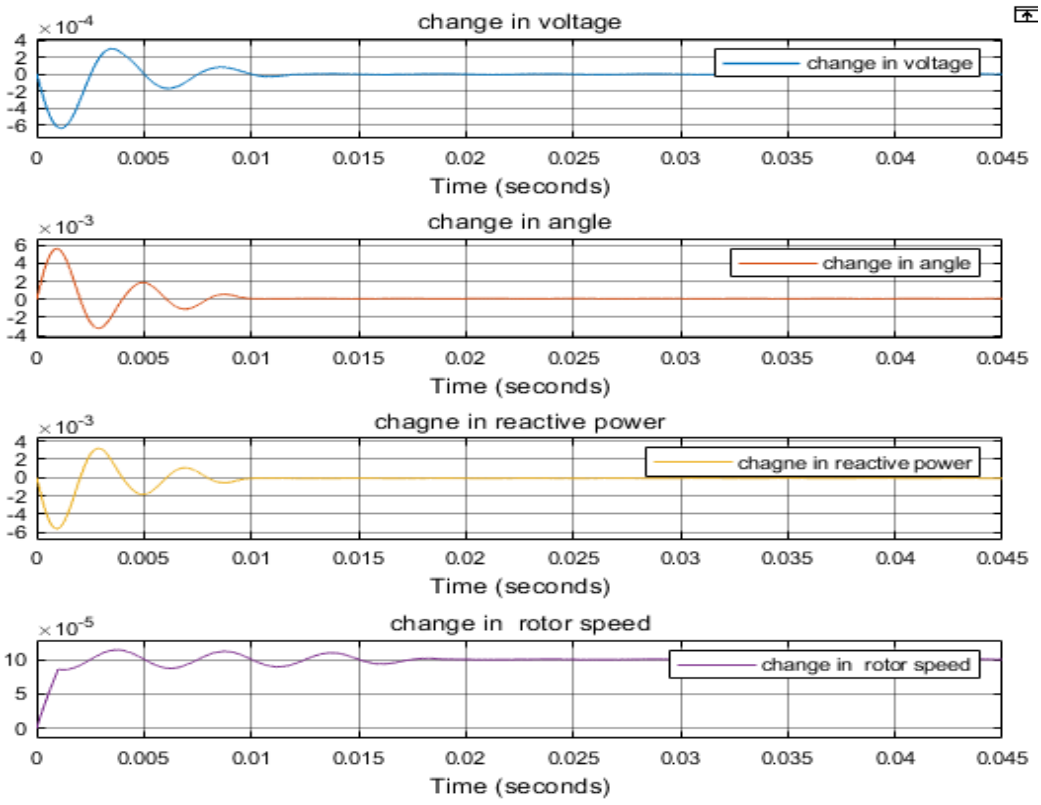

Figure 43. Case 3: Improvement of Transient stability in a hybrid system using PI Controller

4.3.2 Using Fuzzy Logic Controller

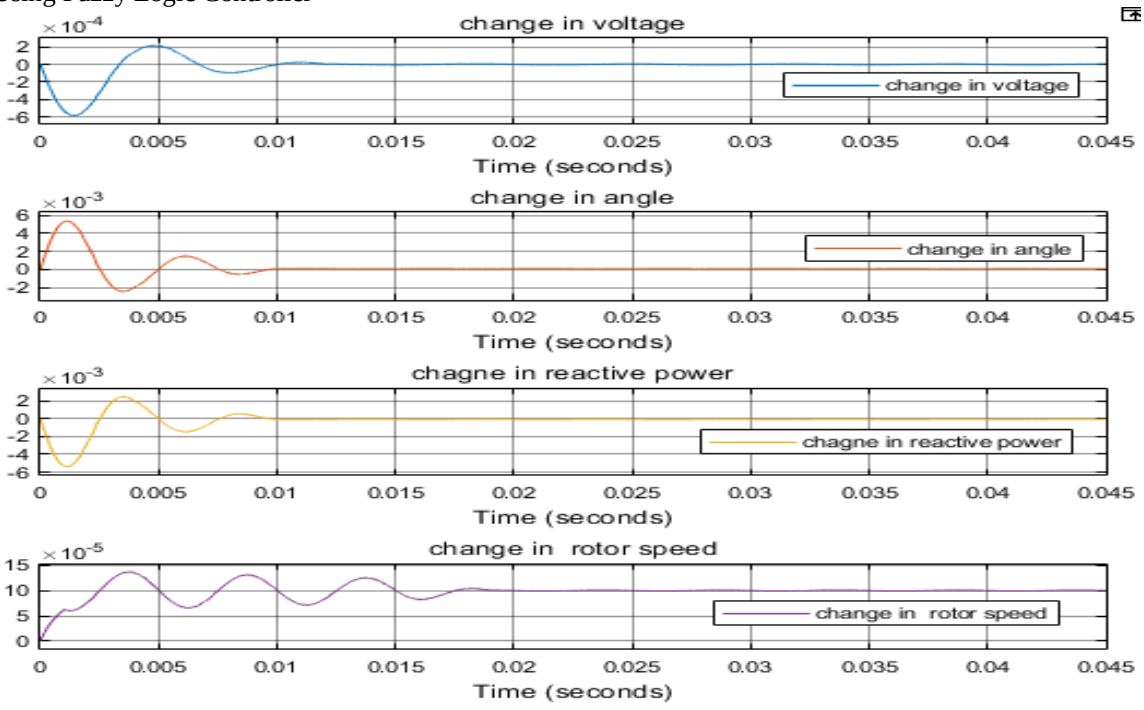

Figure 44. Case 3: Improvement of Transient stability in a hybrid system using Fuzzy Logic Controller

|e-ISSN: 2319-8753, p-ISSN: 2347-6710| www.ijirset.com | Impact Factor: 8.423| A Monthly Peer Reviewed & Refereed Journal |

|| Volume 13, Issue 5, May 2024 ||

| DOI:10.15680/IJIRSET.2024.1305357 |

4.4 Case 4: Improvement of power quality in a hybrid system using ANFIS based DPFC Controller

4.4.1 Output waveforms for distorted micro grid voltage, injected voltage, and compensated grid voltage using ANFIS Controller

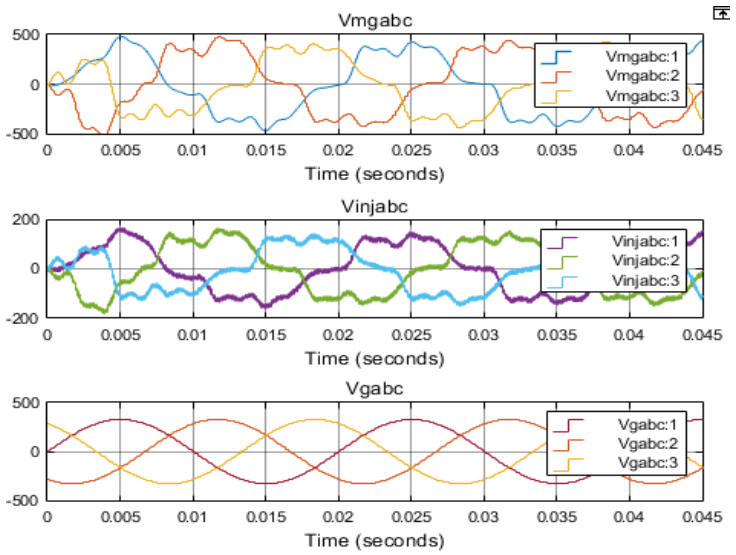

Figure 45. Case 4: Voltage Results using ANFISC; Vmgabc, Vinjabc, Vgabc

4.4.2 Output waveforms for distorted micro grid current, injected current, and compensated grid current.

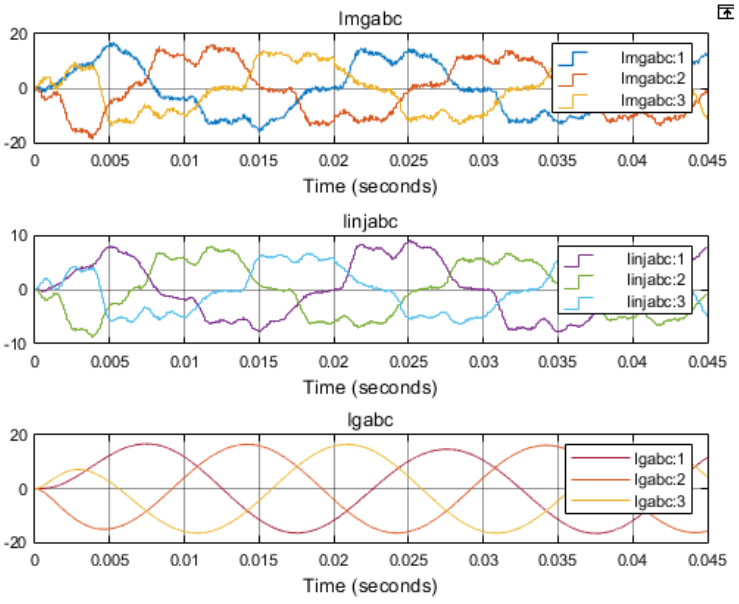

Figure 46. Case 4: Current Results using ANFISC; Imgcabc, linjabc, lgabc

|e-ISSN: 2319-8753, p-ISSN: 2347-6710| www.ijirset.com | Impact Factor: 8.423| A Monthly Peer Reviewed & Refereed Journal |

|| Volume 13, Issue 5, May 2024 ||

| DOI:10.15680/IJIRSET.2024.1305357 |

4.4.3 Output Frequency Results using ANFIS Controller

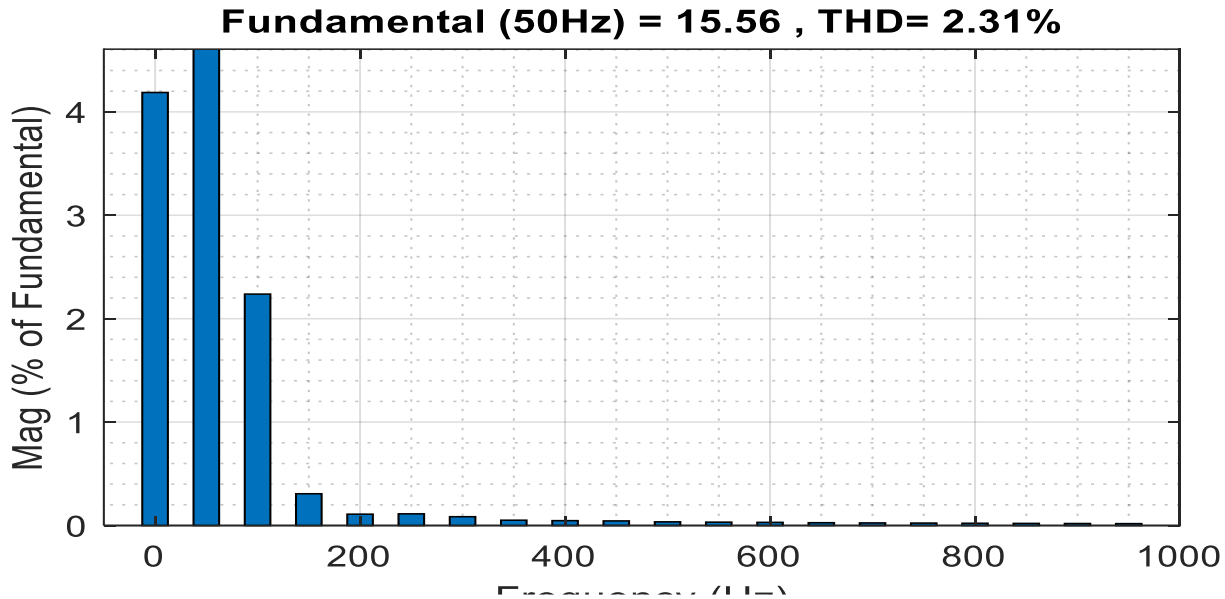

Figure 47. Case 4: Frequency Results; Output using ANFIS controller

4.4 Case 5: Improvement of Transient Stability in a hybrid system using ANFIS based DPFC controller

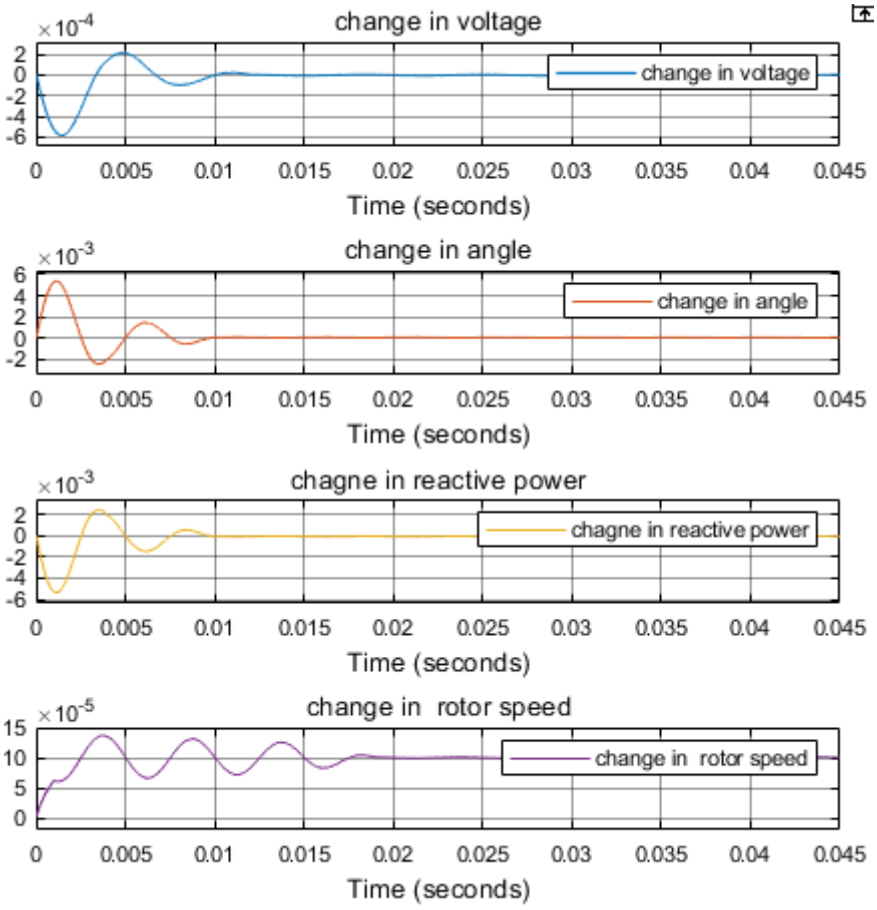

Figure 48. Case 5: Improvement of Transient stability in a hybrid system using ANFIS controller

International Journal of Innovative Research in Science, Engineering and Technology (IJIRSET)

|e-ISSN: 2319-8753, p-ISSN: 2347-6710| www.ijirset.com | Impact Factor: 8.423| A Monthly Peer Reviewed & Refereed Journal |

|| Volume 13, Issue 5, May 2024 ||

| DOI:10.15680/IJIRSET.2024.1305357 |

4.5 Simulation ANFIS results:

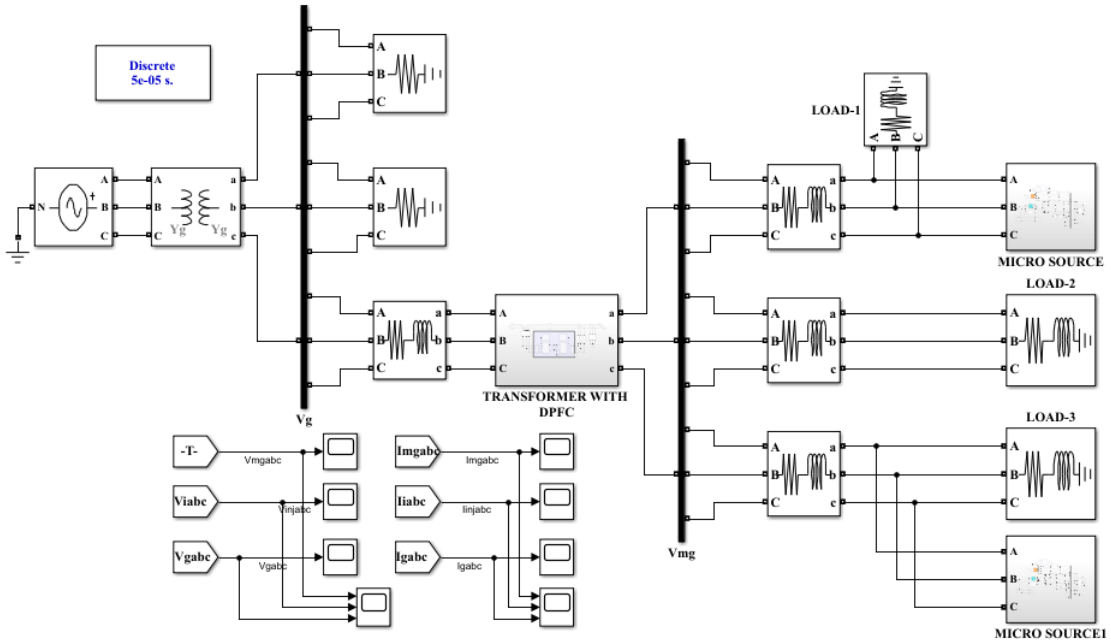

Figure 49. ANFIS Controller Simulation

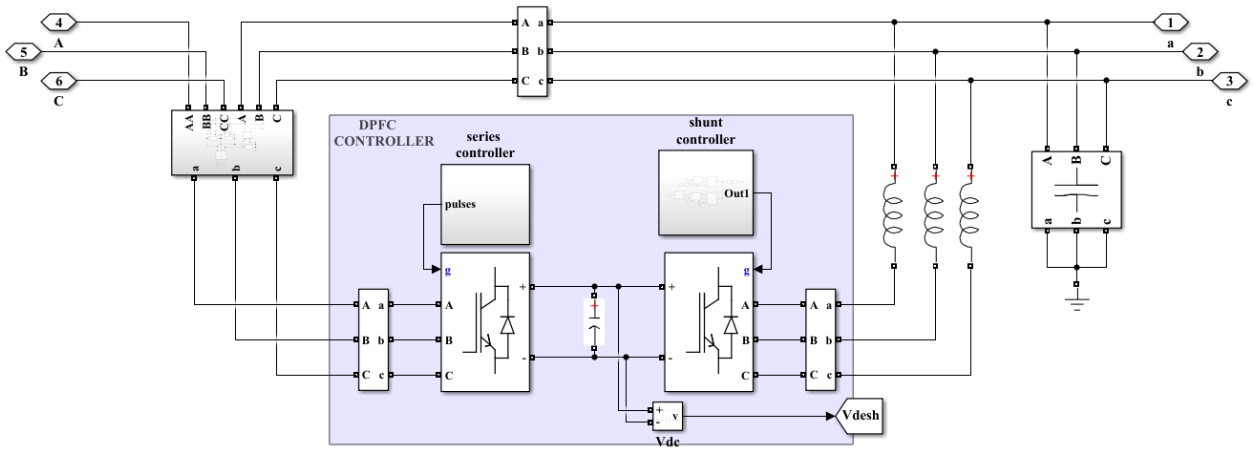

Figure 50. DPFC Controller Simulation

|e-ISSN: 2319-8753, p-ISSN: 2347-6710| www.ijirset.com | Impact Factor: 8.423| A Monthly Peer Reviewed & Refereed Journal |

|| Volume 13, Issue 5, May 2024 ||

| DOI:10.15680/IJIRSET.2024.1305357 |

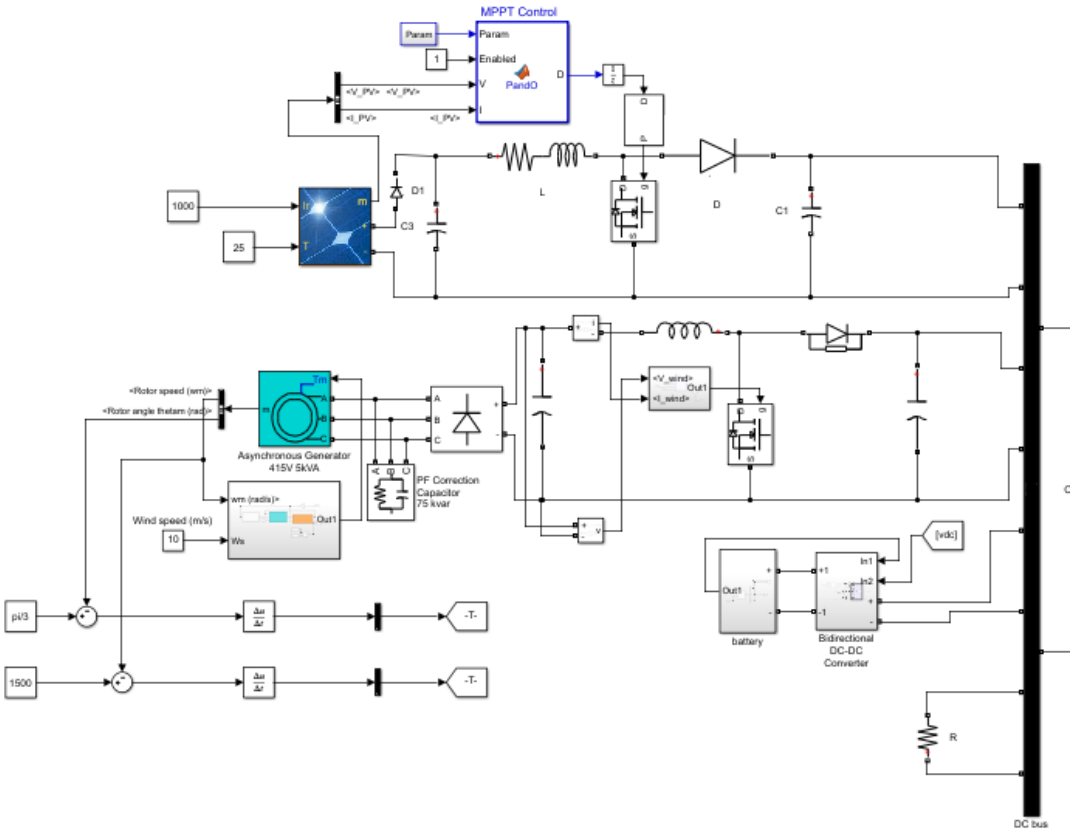

Figure 51. Microgrid Source Simulation

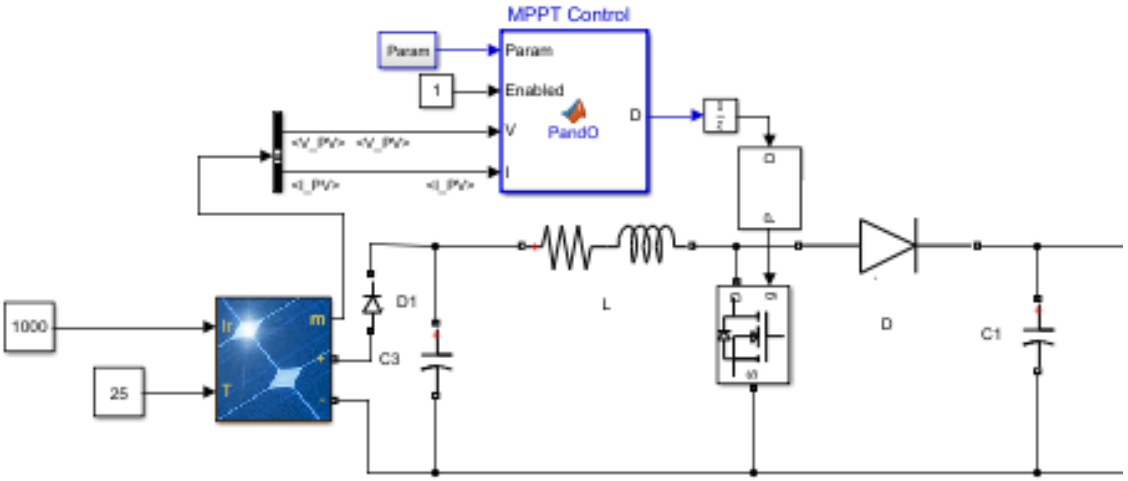

Figure 52. MPPT with Solar Power Demo Simulation

|e-ISSN: 2319-8753, p-ISSN: 2347-6710| www.ijirset.com | Impact Factor: 8.423| A Monthly Peer Reviewed & Refereed Journal |

|| Volume 13, Issue 5, May 2024 ||

| DOI:10.15680/IJIRSET.2024.1305357 |

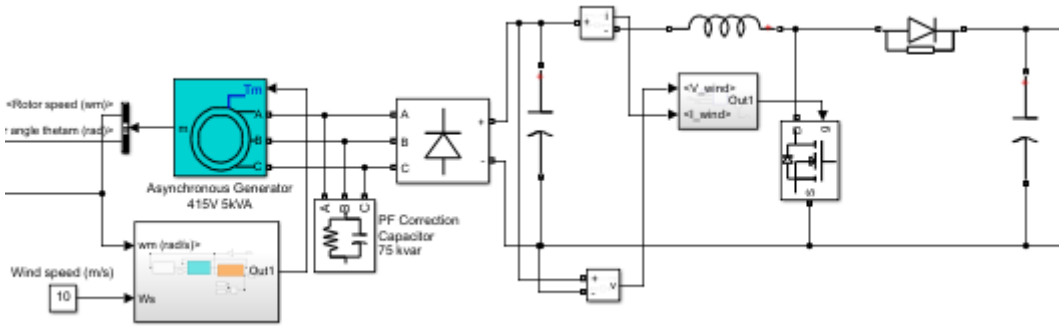

Figure 53. Wind Power Generation Simulation

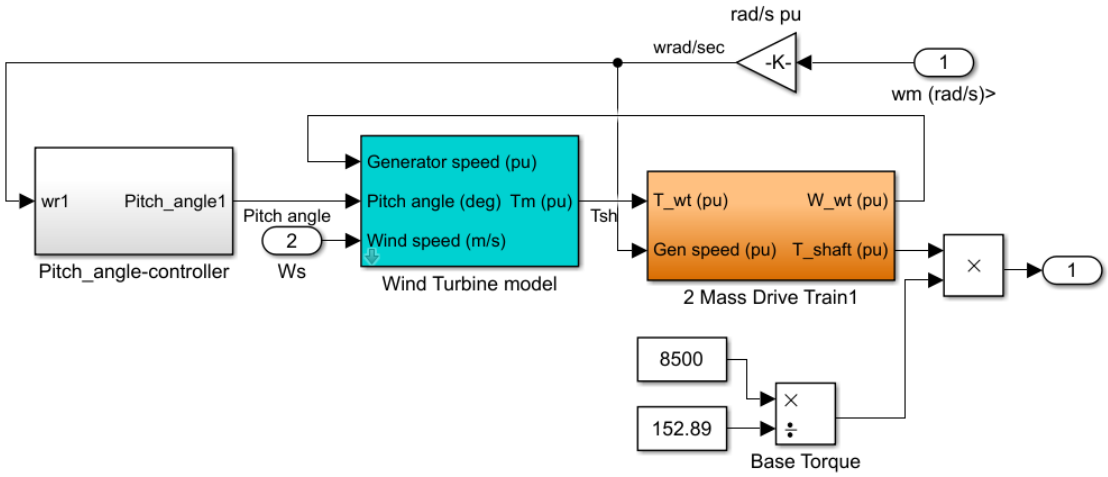

Figure 54. Wind Power Schematic

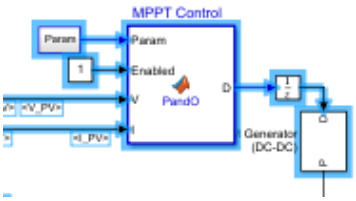

Figure 55. Solar Side MPPT Controller

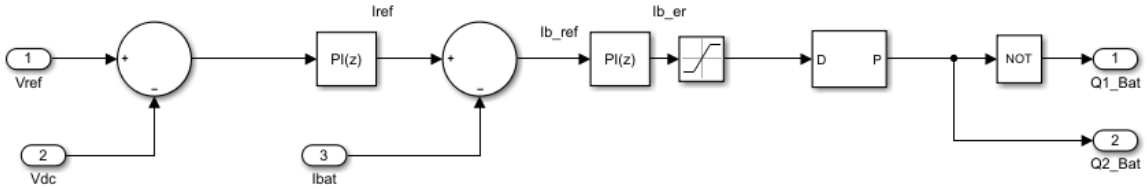

Figure 56. Bidirectional Conversion Controller

International Journal of Innovative Research in Science, Engineering and Technology (IJIRSET)

|e-ISSN: 2319-8753, p-ISSN: 2347-6710| www.ijirset.com | Impact Factor: 8.423| A Monthly Peer Reviewed & Refereed Journal |

|| Volume 13, Issue 5, May 2024 ||

| DOI:10.15680/IJIRSET.2024.1305357 |

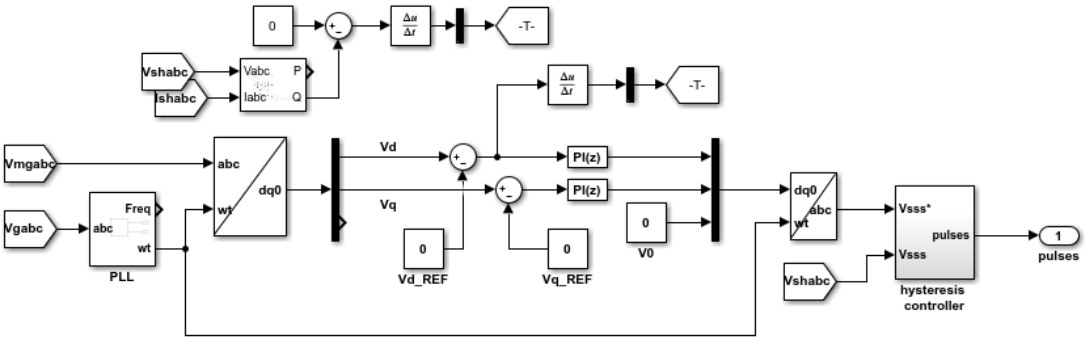

Figure 57. Series Controller Simulation

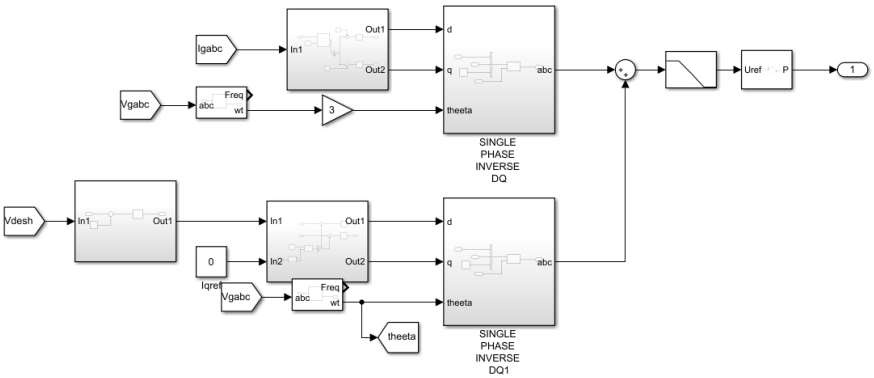

Figure 58. Shunt Controller Simulation

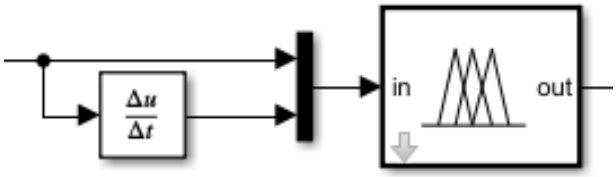

Figure 59. ANFIS Controller

V. SUMMARY AND CONCLUSION

5.1 Conclusion

To sum up, the project "A Novel ANFIS Controller Based Distributed Power Flow Controller for Grid Interfaced Hybrid System" offers a way to enhance the stability and control of hybrid systems that are interfaced with the grid. The advantages of the fuzzy logic controller and the conventional power flow controller are combined in the suggested ANFIS controller. Using a distributed approach lowers the risk of single-point failures and increases system robustness. The suggested technique is successful in enhancing the power flow control and stability of grid-interfaced hybrid systems, according to the results of simulations and experiments.

5.2 Future scope

There are multiple ways to expand the future scope of the "A Novel ANFIS Controller Based Distributed Power Flow Controller for Grid Interfaced Hybrid System" project.

|e-ISSN: 2319-8753, p-ISSN: 2347-6710| www.ijirset.com | Impact Factor: 8.423| A Monthly Peer Reviewed & Refereed Journal |

|| Volume 13, Issue 5, May 2024 ||

| DOI:10.15680/IJIRSET.2024.1305357 |

- Real-time implementation: To verify the suggested method's effectiveness in real-world scenarios, real-time power systems can be used to put it into practice.
- ANFIS controller optimization: By adjusting the model's parameters, the ANFIS controller's performance can be further enhanced.
- Integration with other control techniques: To improve its functionality, the suggested ANFIS controller can be combined with other control techniques.
- Extension to other renewable energy sources: In grid-interfaced hybrid systems, the suggested method can be expanded to regulate and stabilize energy from other renewable energy sources, like solar and wind power.
- Application to large-scale systems: By using the suggested method on large-scale power systems, its scalability can be evaluated.

REFERENCES

1. K. Padmanathan, U. Govindarajan, V. K. Ramachandaramurthy, A. Rajagopalan, N. Pachaivannan, U. Sowmmiya, S. Padmanaban, J. B. Holm-Nielsen, S. Xavier, and S. K. Periasamy, ‘‘A sociocultural study on solar photovoltaic energy system in India: Stratification and policy implication,’’ J. Cleaner Prod., vol. 216, pp. 461–481, Apr. 2019.
2. R. M. Elavarasan, G. Shafiullah, S. Padmanaban, N. M. Kumar, A. Annam, A. M. Vetrichelvan, L. Mihet-Popa, and J. B. Holm-Nielsen, ‘‘A compre-hensive review on renewable energy development, challenges, and policies of leading Indian states with an international perspective,’’ IEEE Access, vol. 8, pp. 74432–74457, 2020.
3. S. Kumar, R. K. Saket, D. K. Dheer, J. B. Holm-Nielsen, and P. Sanjeevikumar, ‘‘Reliability enhancement of electrical power system including impacts of renewable energy sources: A comprehensive review,’’ IET Gener., Transmiss. Distrib., vol. 14, no. 10, pp. 1799–1815, May 2020.
4. I. Masenge and F. Mwasilu, ‘‘Hybrid solar PV-wind generation system coordination control and optimization of battery energy storage system for rural electrification,’’ in Proc. IEEE PES/IAS PowerAfrica, Aug. 2020, pp. 1–5.
5. N. Priyadarshi, S. Padmanaban, M. S. Bhaskar, F. Blaabjerg, and J. B. Holm-Nielsen, ‘‘An improved hybrid PV-wind power system with MPPT for water pumping applications,’’ Int. Trans. Electr. Energy Syst., vol. 30, no. 2, p. e12210, Feb. 2020.
6. S. Padmanaban, K. Nithiyananthan, S. P. Karthikeyan, and J. B. Holm-Nielsen, Microgrids. Boca Raton, FL, USA: CRC Press, 2020.
7. A. Suman, ‘‘Role of renewable energy technologies in climate change adaptation and mitigation: A brief review from Nepal,’’ Renew. Sustain. Energy Rev., vol. 151, Nov. 2021, Art. no. 111524. [Online]. Available: https://www.sciencedirect.com/science/article/pii/ S1364032121008029
8. L. Varshney, A. S. S. Vardhan, S. Kumar, R. Saket, and P. Sanjeevikumar, ‘‘Performance characteristics and reliability assessment of self-excited induction generator for wind power generation,’’ IET, Renew. Power Gener., vol. 15, pp. 1927–1942, 2021.
9. M. Seapan, Y. Hishikawa, M. Yoshita, and K. Okajima, ‘‘Temperature and irradiance dependences of the current and voltage at maximum power of crystalline silicon PV devices,’’ Sol. Energy, vol. 204, pp. 459–465, Jul. 2020. [Online]. Available: https://www.sciencedirect. com/science/article/pii/S0038092X20305089
10. F. Mebrahtu, B. Khan, P. Sanjeevikumar, P. K. Maroti, Z. Leonowicz, O. P. Mahela, and H. H. Alhelou, ‘‘Harmonics mitigation in industrial sector by using space vector PWM and shunt active power filter,’’ in Proc. IEEE Int. Conf. Environ. Electr. Eng., IEEE Ind. Commercial Power Syst. Eur. (EEEIC/I&CPS Europe), Jun. 2020, pp. 1–6.
11. S. Vadi, S. Padmanaban, R. Bayindir, F. Blaabjerg, and L. MihetPopa, ‘‘A review on optimization and control methods used to provide transient stability in microgrids,’’ Energies, vol. 12, no. 18, p. 3582, Sep. 2019.
12. N. Priyadarshi, S. Padmanaban, R. K. Ghadai, A. R. Panda, and R. Patel, ‘‘Advances in power systems and energy management select proceedings of ETAEERE 2020,’’ in Power System and Energy. Springer, 2020, p. 4.
13. E. Sundaram and M. Venugopal, ‘‘On design and implementation of three phase three level shunt active power filter for harmonic reduction using synchronous reference frame theory,’’ Int. J. Electr. Power Energy Syst., vol. 81, pp. 40–47, Oct. 2016.
14. A. Raj, S. R. Arya, and J. Gupta, ‘‘Solar PV array-based DC–DC converter with MPPT for low power applications,’’ Renew. Energy Focus, vol. 34, pp. 109–119, Sep. 2020. [Online]. Available: https://www.sciencedirect. com/science/article/pii/S1755008420300193
15. C. H. Basha and C. Rani, ‘‘Different conventional and soft computing MPPT techniques for solar PV systems with high step-up boost converters: A comprehensive analysis,’’ Energies, vol. 13, no. 2, p. 371, Jan. 2020.
16. J. D. Kumar, K. Mantosh, M. S. Bhaskar, P. Sanjeevikumar, J. B. H. Nielsen, and Z. Leonowicz, ‘‘Investigation studies of DC– DC boost converter with proportional-integral-derivative controller using optimization

|e-ISSN: 2319-8753, p-ISSN: 2347-6710| www.ijirset.com | Impact Factor: 8.423| A Monthly Peer Reviewed & Refereed Journal |

|| Volume 13, Issue 5, May 2024 ||

| DOI:10.15680/IJIRSET.2024.1305357 |

techniques,'' in Proc. IEEE Int. Conf. Environ. Electr. Eng., IEEE Ind. Commercial Power Syst. Eur. (EEEIC/I&CPS Europe), Jun. 2020, pp. 1–5.

17. K. Gulyamov, R. Yunusov, S. Dovudov, B. Sharifov, A. Ghulomzoda, and M. Safaraliev, ''Increase in power of DC/DC converters with increased number of conversion channels,'' in Proc. Ural Smart Energy Conf. (USEC), Nov. 2020, pp. 59–62.
18. N. Hawkins, B. Bhagwat, and M. L. McIntyre, ''Nonlinear current mode control of SCIG wind turbines,'' Energies, vol. 14, no. 1, p. 55, Dec. 2020.
19. A. M. M. dos Santos, L. T. P. Medeiros, L. P. S. Silva, I. D. S. Junior, V. S. de C. Teixeira, and A. B. Moreira, ''Wind power system connected to the grid from squirrel cage induction generator (SCIG),'' in Proc. IEEE 15th Brazilian Power Electron. Conf., 5th IEEE Southern Power Electron. Conf. (COBEP/SPEC), Dec. 2019, pp. 1–6.
20. A. K. S. Tomar, K. K. Gautam, and A. Lodhi, ''Integration of SCIG wind energy conversion systems to the grid,'' Int. J. Eng. Sci. Invention, vol. 9, no. 6, pp. 28–36, 2020.
21. B. B. Adetokun, C. M. Muriithi, and J. O. Ojo, ''Voltage stability analysis and improvement of power system with increased SCIG-based wind system integration,'' in Proc. IEEE PES/IAS PowerAfrica, Aug. 2020, pp. 1–5.
22. M. Xu, L. Wu, H. Liu, and X. Wang, ''Multi-objective optimal scheduling strategy for wind power, PV and pumped storage plant in VSC-HVDC grid,'' J. Eng., vol. 2019, no. 16, pp. 3017–3021, Mar. 2019.
23. P. Manoharan, U. Subramaniam, T. S. Babu, S. Padmanaban, J. B. Holm-Nielsen, M. Mitolo, and S. Ravichandran, ''Improved perturb and observation maximum power point tracking technique for solar photovoltaic power generation systems,'' IEEE Syst. J., vol. 15, no. 2, pp. 3024–3035, Jun. 2021.
24. M. H. Reza and M. A. Shobug, ''Efficiency evaluation of P&O MPPT technique used for maximum power extraction from solar photovoltaic system,'' in Proc. IEEE Region Symp. (TENSYMP), Jun. 2020, pp. 1808–1811.
25. A. Ali, K. Almutairi, S. Padmanaban, V. Tirth, and S. Algarni, ''Investigation of MPPT techniques under uniform and non-uniform solar irradiation condition—A retrospection,'' IEEE Access, vol. 8, pp. 127368–127392, 2020.
26. G. S. Chawda, A. G. Shaik, O. P. Mahela, S. Padmanaban, and J. B. Holm-Nielsen, ''Comprehensive review of distributed facts control algorithms for power quality enhancement in utility grid with renewable energy penetration,'' IEEE Access, vol. 8, pp. 107614–107634, 2020.
27. A. Sen, A. Banerjee, and H. Nannam, ''A comparative analysis between two DPFC models in a grid connected hybrid solar-wind generation system,'' in Proc. IEEE Int. Conf. Power Electron., Smart Grid Renew. Energy (PESGRE), Jan. 2020, pp. 1–6.
28. X. Zhai, A. Tang, X. Zou, X. Zheng, and Q. Xu, ''Research on DPFC capacity and parameter design method,'' in Proc. IEEE Int. Conf. Inf. Technol., Big Data Artif. Intell. (ICIBA), vol. 1, Nov. 2020, pp. 978–982.
29. J. H. Woo, L. Wu, S. M. Lee, J.-B. Park, and J. H. Roh, ''D-STATCOM d-q axis current reference control applying DDPG algorithm in the distribution system,'' IEEE Access, vol. 9, pp. 145840–145851, 2021.
30. G. Balasubramani, V. Thangavelu, M. Chinnusamy, U. Subramaniam, S. Padmanaban, and L. Mihet-Popa, ''Infrared thermography-based defects testing of solar photovoltaic panel with fuzzy rule-based evaluation,'' Energies, vol. 13, no. 6, p. 1343, Mar. 2020.
31. S. V. K. Arun, U. Subramaniam, S. Padmanaban, M. S. Bhaskar, and D. Almakhles, ''Investigation for performances comparison PI, adaptive PI, fuzzy speed control induction motor for centrifugal pumping application,'' in Proc. IEEE 13th Int. Conf. Compat., Power Electron. Power Eng. (CPE-POWERENG), Apr. 2019, pp. 1–6.
32. B. Alshammari, R. B. Salah, O. Kahouli, and L. Kolsi, ''Design of fuzzy TS-PDC controller for electrical power system via rules reduction approach,'' Symmetry, vol. 12, no. 12, p. 2068, Dec. 2020.
33. D. Sharma and N. K. Yadav, ''Lion algorithm with Levy update: Load frequency controlling scheme for two-area interconnected multi-source power system,'' Trans. Inst. Meas. Control, vol. 41, no. 14, pp. 4084–4099, Oct. 2019, doi: 10.1177/0142331219848033.
34. M. Yazdani and F. Jolai, ''Lion optimization algorithm (LOA): A nature inspired metaheuristic algorithm,'' J. Comput. Des. Eng., vol. 3, no. 1, pp. 24–36, 2016.
35. [Online]Available:https://www.sciencedirect.com/science/article/pii/S2288430015000524
36. R. Shankar, ''Lion algorithm-based load frequency control for interconnected power system in coordination with UPFC and electric vehicle,'' in Proc. Int. Conf. Recent Innov. Electr., Electron. Commun. Eng. (ICRIEECE), Jul. 2018, pp. 575–580.

INTERNATIONAL STANDARD SERIAL NUMBER INDIA

INNO SPACE SJIF Scientific Journal Impact Factor

doi cross ref

निस्केयर NISCAIR

INTERNATIONAL JOURNAL OF INNOVATIVE RESEARCH

IN SCIENCE | ENGINEERING | TECHNOLOGY

9940 572 462 6381 907 438 ijirset@gmail.com

www.ijirset.com

Scan to save the contact details